Late Quaternary deformation in the western extension of the North Anatolian Fault (North Evia, Greece): Insights from very high-resolution seismic data (WATER surveys)

Fabien Caroir, Frank Chanier, Virginie Gaullier, Dimitris Sakellariou, Julien Bailleul, Agnès Maillard, Fabien Paquet, Louise Watremez, Olivier Averbuch, Fabien Graveleau, et al.

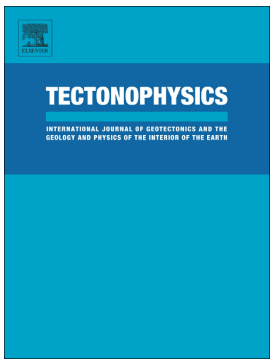

Late Quaternary deformation in the western extension of the North Anatolian Fault (North Evia, Greece): Insights from very high-resolution seismic data (WATER surveys)

Fabien Caroir, Frank Chanier, Virginie Gaullier, Dimitris Sakellariou, Julien Bailleul, Agnès Maillard, Fabien Paquet, Louise Watremez, Olivier Averbuch, Fabien Graveleau, Jacky Ferrière

PII: S0040-1951(23)00436-5

DOI: https://doi.org/10.1016/j.tecto.2023.230138

Reference: TECTO 230138

To appear in: *Tectonophysics*

Received date: 19 January 2023

Revised date: 13 November 2023

Accepted date: 14 November 2023

Please cite this article as: F. Caroir, F. Chanier, V. Gaullier, et al., Late Quaternary deformation in the western extension of the North Anatolian Fault (North Evia, Greece): Insights from very high-resolution seismic data (WATER surveys), *Tectonophysics* (2023), https://doi.org/10.1016/j.tecto.2023.230138

Late Quaternary deformation in the western extension of the North Anatolian Fault (North Evia, Greece): insights from very high-resolution seismic data (WATER surveys)

Authors: Fabien Caroir[1], Frank Chanier[1], Virginie Gaullier[1], Dimitris Sakellariou[2], Julien Bailleul[3], Agnès Maillard[4], Fabien Paquet[5], Louise Watremez[1], Olivier Averbuch[1], Fabien Graveleau[1] and Jacky Ferrière[1]

1) Univ. Lille, CNRS, Univ. Littoral Côte d'Opale, IRD, UMR8187, LOG, Laboratoire d'Océanologie et de Géosciences, F59000 Lille, France,

2) HCMR, Hellenic Centre for Marine Reasearch, Anavyssos, Greece,

3) U2R7511, Bassins-Réservoirs-Ressources (B2R), Geosciences department, UniLaSalle – University of Picardie Jules Verne, 60026, Beauvais, France,

4) Géosciences Environnement Toulouse (GET) -- Institut de Recherche pour le Développement, Université Paul Sabatier - Toulouse 3, Observatoire Midi-Pyrénées, CNRS : UMR5563, France,

5) DGR-GBS Bureau de Recherches Géologiques et Minières (BRGM), France

Abstract

Since the Pliocene, rift basins have developed in the North Evia region at the south-western extension of the North Anatolian Fault. North Evia, therefore, is a key area for investigating Plio-Quaternary deformation within the diffuse Anatolian-Aegean–Eurasian plate boundary. In this study, we present a detailed map of offshore faults in the North Evia region based on three seismic reflection surveys: an airgun (2004) and two very high-resolution Sparker (2017 and 2021) single-channel surveys. Careful and systematic interpretation of these datasets revealed i) the identification of a new basin (Skiathos Basin) located at the western extension of the North Anatolian Fault and ii) two main fault sets striking oblique to the active N–S-directed extension. The seismicity analysis of the study area reveals pure strike-slip displacements along faults previously identified as normal. The NW–SE-striking faults bordering the North Evia Gulf rift are characterised by left-lateral displacements, and the NE–SW faults present dextral focal mechanisms, following the kinematic character of the North Anatolian Fault. We show that dextral strike-slip deformation recently occurred (in the late Quaternary) in the south-western extension of the North Anatolian Fault, suggesting the significant role of this fault system in the complex structural development of the North Evia region.

Keywords: North Evia region, North Anatolian Fault, Rifting, Aegean Sea, Strike-slip faults

1. Introduction

The Eastern Mediterranean and Aegean regions are an active tectonic zone (*e.g.*, McKenzie, 1978; Dewey and Sengör, 1979; Le Pichon and Angelier, 1979; 1981; Roberts and Jackson, 1991; Taymaz et al, 1991; Jackson, 1999; Armijo et al, 1996; 1999; Hatzfeld, 1999; McClusky *et al.*, 2000; Hollenstein *et al.*, 2008; Müller *et al.*, 2013) consisting of numerous onshore and offshore tectonic structures that have been developed over a complex geological history. This tectonic history involved Late Cretaceous to early Tertiary orogenesis (*i.e.* the Hellenides–Taurides orogenic system) and subsequent extensional collapse that led to the present "basin-and-range" topography of eastern Greece and western Turkey, and the development of the Aegean basin in the core of the former orogenic belt (Figure 1, *e.g.*, Gauthier and Brun, 1994; van Hinsbergen *et al.*, 2005a; Jolivet and Brun, 2010; Jolivet *et al.*, 2013; Menant *et al.*, 2016; Kilias, 2021).

Two major features associated with the active tectonics of the Aegean are the East and North Anatolian Faults (EAF and NAF, Figure 1-A), which accommodate the westward extrusion of the Anatolian block (*e.g.*, Dewey and Sengör, 1979; Sengör, 1979; Hubert-Ferrari *et al.*, 2002; 2003). Coupled with the distributed extension triggered during the Miocene, the North Anatolian Fault, has greatly modified the northern part of the Aegean Sea. Previous studies have suggested that the northern branch of the North Anatolian Fault terminates in the North Aegean Trough (NAT, Figure 1-A, *e.g.*, Armijo *et al.*, 1999; Papanikoalou *et al.*, 2006; Sakellariou *et al.*, 2016). The North Anatolian Fault initially developed in eastern Turkey 11–13 Myr ago (Sengör *et al.*, 2005) and propagated to western Turkey 5–2.5 Myr ago (Armijo *et al.*, 1999; Le Pichon *et al.*, 2016). During this westward propagation, the North Anatolian Fault became localised. The propagation of the NAF into the North Aegean Trough was established during the early–middle Pleistocene. In the western extension of the North Aegean Trough, NE–SW-striking faults (akin to the North Anatolian Fault) have been found (Kiratzi, 2002; Palyvos et al., 2006), whereas the deformation in this area is mainly located along the WNW–ESE and NW–SE-striking faults belonging to the Sperchios–North Evia Gulf rift (Figures 1-B and 2).

The Sperchios–North Evia Gulf rift is located in the eastern part of Central Greece administrative district and is one of the main intra-continental rifts in Greece (Figure 1). This 140-km-long basin separates Central Greece from northern Evia and Mount Othrys (Figure 2), with a maximum width of 25 km. GPS geodetic surveys (McClusky *et al.*, 2000; Hollenstein *et al.*, 2008; Chousianitis *et al.*, 2013; Müller *et al.*, 2013) have revealed active extension in

the North Evia region, with an extension rate ranging from 1 to 3 mm/yr, mainly accommodated by the normal faults of the Kamena Vourla–Arkitsa Fault System (Chousianitis *et al.*, 2013). The North Evia region (*i.e.* the North Evia Gulf, the island of North Evia, the Oreoi and Artemision Channels, and the Skopelos Basin, Figure 2) is also characterised by seismic activity, with events of Mw > 6 recorded in the Pagasitikos Gulf (Drakos *et al.*, 2001), along the Atalanti Fault (Ganas *et al.*, 1998; Novikova *et al.*, 2017) and in the surroundings of the Lichades Peninsula. This study presents a compilation of these seismic events.

Paleomagnetic data reveal clockwise rotations during the last 3 Myr in the North Evia domain, whereas in the north, Thessaly appears stable in terms of rotations over this timescale (Kissel *et al.*, 1989; Kondopoulou and Caputo, 1997; Bradley *et al.*, 2013; van Hinsbergen *et al.*, 2020). This difference is important for understanding the deformation of the area beyond the western termination of the North Anatolian Fault (*i.e.* the North Evia region and the Corinth rift). On a broader level, this key area can be used to evaluate the role of the structures inherited from the complex geological history of Greece and the rift geometries in the context of the African slab retreat. The purpose of this study is to better understand recent deformation in the North Evia region and integrate it into the regional tectonic evolution of the north-western Aegean Sea. Compared with the Corinth rift, which has been the focus of numerous seismological, sedimentary, and structural investigations (*e.g.*, Collier and Dart, 1991; Armijo *et al.*, 1996; Roberts, 1996; Sorel, 2000; Goldsworthy and Jackson, 2001; Moretti *et al.*, 2003; Flotté *et al.*, 2005; Bernard *et al.*, 2006; Ford *et al.*, 2007; Leeder *et al.*, 2008; 2012; Jolivet *et al.*, 2010; Nixon *et al.*, 2016), the North Evia region has been less thoroughly analysed. As it is located southwest of the western termination of the North Anatolian Fault (Figure 1-B), it is crucial to precisely determine the active tectonics and plate boundaries between the Eurasian and Anatolian-Aegean plates (Figure 1-A). This plate boundary context, which includes intense seismic activity, highlights the necessity of improving our understanding of the deformation mode and seismic hazards. This can be achieved through the characterisation of fault geometries and kinematics. To achieve these objectives, two very high-resolution Sparker seismic surveys, WATER 1 and 2 (2017 and 2021), were conducted in the North Evia Gulf, the Oreoi and Artemision Channels, and the Skopelos Basin (Figure 3). In addition, we also analysed brittle deformation in North Evia.

2. Geodynamic and tectonic setting

2.1. General tectonic setting

The Hellenides resulted from a complex geodynamic history, which involved a succession of divergent and convergent episodes since the Jurassic of various crustal domains (Pelagonian, Maliac, Pindos, Gavrovo-Tripolitza, Figure 1-B). The Maliac and Vardar oceanic domains opened during the Triassic and early Jurassic (Ferrière, 1972, 1974, 1976; Hynes *et al.*, 1972; Smith *et al.*, 1975). During the Late Jurassic, intra-oceanic subduction developed at the mid-oceanic ridge, leading to the obduction of Maliac ophiolitic units above the Pelagonian continental crust (Mountrakis, 1987; Sharp and Robertson, 2006; Kilias *et al.*, 2010; Ferriere *et al.*, 2012; 2016; Schmid *et al.*, 2019; Porkoláb *et al.*, 2019). The Pelagonian unit is a fragment of a former continental block (the Cimmerian block) composed of Palaeozoic or older crystalline rocks, above which carbonates and volcano-sedimentary sequences were deposited during the Triassic and Jurassic (Guernet, 1971; Clement, 1983; Baud *et al.*, 1991; Pe-Piper and Panagos, 1989; Angelini *et al.*, 1992). The Pindos basin comprises carbonate and clastic stratigraphic series from the Triassic to the Eocene. While oceanic crust has not been observed in the Pindos basin, some authors have suggested that part of this basin was formed by oceanic spreading during the Jurassic (Dercourt, 1970; Thiébault, 1982; Vergely, 1984; Robertson *et al.*, 1991; Saccani *et al.*, 2004; Dilek *et al.*, 2008). According to this hypothesis, ophiolite nappes, which have been thrust over Pelagonian units, may come partly from Pindos and not solely from the Maliac domain (Vergely, 1984; Mountrakis, 1987; Sharp and Robertson, 1998; Beccaluva *et al.*, 2005; Robertson, 2006; Saccani *et al.*, 2008). The Hellenides can be divided into two main zones: 1) the Internal Zones to the east and 2) the External Zones to the west. A major fault zone separates them, the Internal Zones Thrust Front (IZTF, Figure 1). The iInternal Zones are usually defined by their relationship with the Late Jurassic obduction event.

Based on mantle tomography, current geodynamic models suggest that the present active subduction, observed along the Mediterranean ridge (Figure 1-A) between the Eurasian and African plates, developed as part of a unique slab below the Aegean domain submitted to a progressive long-term retreat (van Hinsbergen *et al.*, 2005b; Brun and Faccenna, 2008; Brun and Sokoutis, 2010; Jolivet and Brun, 2010; Jolivet *et al.*, 2013; Brun *et al.*, 2016; Menant *et al.*, 2016). This subduction likely initiated during Jurassic times along the Vardar trench (Sengör and Yilmaz, 1981; Dercourt *et al.*, 1986; Ricou *et al.*, 1986; Ricou *et al.*, 1994; Ferrière and Stais, 1994, 1995; Ferrière *et al.*, 2016), and migrated towards the southwest as

the plunging lithospheric slab progressively delaminated and submitted to a general retreat. This retreat allowed the exhumation of the subducted crustal slices (*e.g.*, Brun *et al.*, 2016). During the Late Cretaceous and Cenozoic, the compressional regime induced by the subduction process was responsible for accretion and nappe stacking, leading to the formation of the Hellenides mountain belt (Le Pichon and Angelier, 1979; Jolivet, 2003; van Hinsbergen *et al.*, 2005b; 2005c; Jolivet and Brun, 2010; Brun *et al.*, 2016; Menant *et al.*, 2016; Kilias, 2021). The southward migration of the subduction front and associated slab roll-back may have induced a major upwelling of the asthenosphere at the subduction corner. This led to a back-arc extensional regime within the upper plate and the thinning of the Aegean crust (*e.g.*, Jolivet *et al.*, 2013; Brun *et al.*, 2016), evidenced by shallow Moho depths (Tiberi *et al.*, 2001; Zelt *et al.*, 2005; Sachpazi *et al.*, 2007; Makris *et al.*, 2013; Faucher *et al.*, 2021). The oldest extension markers are observed in the Rhodope massif and consist of Metamorphic Core Complexes, whose exhumation started in the Eocene and lasted until the middle Miocene (Brun and Sokoutis, 2007; Burchfiel *et al.*, 2008; Burg, 2012). To the south, Eocene and Oligocene extension markers have also been documented in Thessaly and the Sporades Islands (Lips *et al.*, 1998; Walcott, 1998; Brokolab *et al.*, 2019; 2020). Farther south, an extensional phase occurred from the late Eocene to the early Miocene in the Cyclades, leading to the exhumation of more Metamorphic Core Complexes (Bonneau, 1984; Faure and Bonneau, 1988; Gautier and Brun, 1994; Jolivet *et al.*, 1994, 2003, 2004; Vanderhaeghe and Teyssier, 2001; van Hinsbergen *et al.*, 2005b; Ring *et al.*, 2010; Grasemann *et al.*, 2012). Since the middle Miocene (~13 Ma), the style of extension, which was previously relatively localised, became more distributed within the Aegean region (Brun *et al.*, 2016). This change in the extensional regime is considered to be caused by an increase in the slab retreat rate (Brun *et al.*, 2016). This rate accelerated during the Miocene from approximately 0.6 to 3.2 cm/yr (Brun *et al.*, 2016); the latter is similar to current estimates for the velocity of the Aegean block based on kinematic modelling (Ganas and Parsons, 2009). Ganas and Parsons (2009) highlighted that the Nubian plate is moving northward at c. 0.5 cm/yr relative to Eurasia, whereas the Aegean block is moving southward at c. 3.3 cm/yr relative to Eurasia. According to Ganas and Parsons (2009), this velocity difference shows a nearly passive Nubian slab overridden by the faster Aegean block.

2.2. Aegean region

Two main factors control the current geodynamics of the eastern Mediterranean: 1) the northward subduction of the African plate and 2) the westward extrusion of the Anatolian-

Aegean microplate (Figure 1-A). The latter is accommodated to the east, along the East Anatolian Fault (Figure 1-A), the boundary between the Anatolian-Aegean and Arabian plates. To the north, the North Anatolian Fault partially accommodates this extrusion (Figure 1-A), which is a major dextral strike-slip fault (Ketin, 1948). The North Anatolian Fault is the plate boundary between the Eurasian and Anatolian-Aegean plates. The Aegean region has classically been defined as a non-deformed rigid block moving toward the southwest (fixed Eurasia) at a rate of approximately 30 mm/yr (Figure 1-A, Clarke *et al.*, 1998; Reilinger *et al.*, 2006; Floyd *et al.*, 2010; Le Pichon and Kreemer, 2010; Reilinger *et al.*, 2010; Royden and Papanikolaou, 2011). In contrast, Anatolia moves westwards with respect to Eurasia at a rate of 24 mm/yr. Furthermore, recent geological and structural data indicate significant deformation within the Aegean region (Sakellariou and Tsampouraki-Kraounaki, 2019 and references therein).

The north-western part of the Aegean region is characterised by the Central Hellenic Shear Zone (CHSZ, Figure 1-A, Sengör, 1979; Sengor and Canitez, 1982), which extends from southern Thessaly to Peloponnese and from the Kefalonia Transform Fault (KTF, Figure 1-A) to the North Aegean Trough (Figure 1-A). The existence of the Central Hellenic Shear Zone may be anticipated in terms of plate tectonics and crustal block models (*e.g.* Mercier, 1981; Armijo *et al*., 1999; Goldsworthy *et al.*, 2002). However, no geological data on the southern coast of the North Evia Gulf supports its existence (Ganas, 1997; Galanakis *et al.*, 1998; Roberts and Ganas, 2000). The Central Hellenic Shear Zone constitutes a major extensional region, characterised by 20–25 mm/yr cumulate dextral slip rates determined from GPS data (Le Pichon *et al.*, 2016) and clockwise rotations of about 40° between 15–13 Ma and 8 Ma, and 10° since 4 Myr (Kissel *et al.*, 2003; van Hinsbergen *et al.*, 2005c, 2010). The Sperchios–North Evia Gulf rift belongs to the Pliocene structures that accommodate this extensional tectonic regime (Figure 2).

2.3. North Anatolian Fault

The North Anatolian Fault is a major ~1200-km-long dextral strike-slip fault separating the Anatolian-Aegean plate from the Eurasian plate (Figure 1-A). This plate boundary started its westward propagation between 11 and 13 Myr ago from eastern Turkey (Şengör *et al.*, 2005). It reached the Marmara Sea (Ma in Figure 1A) approximately 5 Myr ago (Armijo *et al.*, 1999; Le Pichon *et al.*, 2014) and started its western propagation through the Aegean Sea. Its current slip rate is ~24 mm/yr, determined by GPS horizontal velocity and measurements of geomorphological offsets (McClusky *et al.*, 2000; Hubert-Ferrari *et al.*,

2002). The eastern termination of the NAF is located at the Karliova triple junction (Kar in Figure 1A), where it connects with the East Anatolian Fault. However, the geometry and timing of its western termination within the Aegean are still under discussion.

The present-day western termination of the North Anatolian Fault in the Aegean Sea is divided into two main branches (*e.g.* McKenzie, 1978; Kreemer *et al.*, 2004; Papanikolaou *et al.*, 2019). The southern branch runs south of the Marmara Sea and ends within the Skyros Basin (SkB in Figure 1A), and the northern branch propagates westwards of the Marmara Sea, through the north Aegean Sea towards the NE–SW-striking North Aegean Trough (NAT in Figure 1A). This northern branch constitutes the north-western Eurasia–Anatolia plate boundary (McKenzie, 1970, 1972, 1978; Brunn *et al.*, 1976; Dewey and Sengör, 1979; Sengör, 1979; Le Pichon and Angelier, 1979, 1981; McKenzie and Jackson, 1983; Taymaz *et al.*, 1991; Armijo *et al.*, 1999). As the North Evia region is located southwest of this northern branch, the main plate boundary, this study focuses on the branch that runs along the south-eastern border of the North Aegean Trough (Roussos and Lyssimachou, 1991; Beniest *et al.*, 2016; Sakellariou *et al.*, 2016; Ferentinos *et al.*, 2018, Porkoláb *et al.*, 2023; Rodriguez *et al.*, 2023). The development and localisation of the northern branch of the North Anatolian Fault along the North Aegean Trough is considered to be as young as the middle Pleistocene, starting at about 430 ka (Ferentinos *et al.*, 2018, Rodriguez *et al.*, 2023), and may be as young as c. 100–200 ka on its southern tip along Alonissos Island (Porkoláb *et al.*, 2023).

The North Aegean Trough developed earlier than the northern branch of the North Anatolian Fault, mainly during the Neogene, in response to the N–S extensional deformation of the North Aegean Sea. Many of these early extensional structures were reactivated during the Pleistocene coevally with the propagation of the North Anatolian Fault (Roussos and Lyssimachou, 1991; Beniest *et al.*, 2016, Porkolàb *et al.*, 2023; Rodriguez *et al.*, 2023). The propagation of the North Anatolian Fault formed a horsetail-shaped structure that ends against a large NW–SE-striking normal fault, perpendicular to the westernmost segment of the active North Anatolian Fault along Alonissos Island (*e.g.*, Sakellariou *et al.*, 2016; Porkolàb *et al.*, 2023). Therefore, because no major structures have been identified to the southwest, the North Anatolian Fault is widely considered to end in this area of the Sporades, north of Skopelos Island (*e.g.*, Beniest *et al.*, 2016, Le Pichon *et al.*, 2016; Sakellariou *et al.*, 2016; Ferentinos *et al.*, 2018).

However, some related NE–SW dextral strike-slip structures have also been reported on Alonissos Island (Porkolàb *et al.*, 2023), and further south within the western extension of

the North Aegean Trough, in the North Evia region. These features, which suggest some incipient "North Anatolian Fault-related" deformation, can be morphological, such as the N070E orientation of the Oreoi and Artemision Channels or the Nileas Depression across Evia Island (Figure 2), or structural, such as the Prokopi–Pilion Fault Zone (PPFZ), the Kechriae Fault Zone (KEFZ) bordering the Nileas Depression in Evia, and the Hyampolis Fault Zone (HFZ) in its south-western extension, mainland Greece (see Figure 2 for structure locations). The structural features are often interpreted from morphological characteristics (*e.g.*, Palyvos *et al.*, 2006).

Some seismological studies have outlined the development of some strike-slip and transtensional accommodation of the stress field between the North Aegean Trough and the Corinth Rift, *i.e.* across the North Evia region (Papoulia *et al.*, 2006). Moreover, based on a detailed micro-seismicity study, Kiratzi (2002) has also reported active strike-slip deformation determined from earthquake focal mechanisms in this region. Consequently, even if most of the recent deformation associated with the North Anatolian Fault ends north of Skopelos Island, some active distributed strike-slip deformation must be considered in the North Evia region.

2.4. The North Evia region

The North Evia region, located between Central Greece and the North Aegean Sea, includes the Maliakos Gulf (MG), the North Evia Gulf (NEG) rift basin, the Oreoi and Artemision Channels, the Pagasitikos Gulf, the Skopelos Basin and adjacent land areas, such as Evia Island and eastern central continental Greece (Figure 2). The topography in this part of Greece has very high contrast, including many mountains (Figure 2) with peaks over 1000 metres above sea level, such as Parnassos (up to 2460 m high), Othrys (1726 m), Kallidromon (1399 m), and Kandili (1246 m), which mainly expose the pre-Neogene basement (Pelagonian, Maliac, and Parnassos series).

The offshore areas include two bathymetric lows: the Central Basin (CB) of the North Evia Gulf and the Skopelos Basin (Figure 2). The Central Basin, which reaches a depth of 440 m water depth, is currently fed by several canyons mainly located on its southern and western slopes. The Skopelos Basin is located in the Aegean Sea, off the mouth of the Artemision Channel, north of Evia Island and south of Skopelos Island. It has a triangular shape and is the deepest area within the investigated region, with a water depth of approximately 1050 m. These deep basins are connected through the shallow Oreoi and Artemision Channels, which

form the Oreoi–Artemision Channel. This pair of connected marine channels is only 20 to 80 m deep and emerged during lower sea-level intervals, that is, during the Last Glacial Maximum (Van Andel and Perissoratis, 2006).

Regarding the active deformation of this region, geodetic studies from GPS data (McClusky *et al.*, 2000; Pérouse *et al.*, 2012; Müller *et al.*, 2013) show significant N–S extension between the Chalkidiki Peninsula and Central Greece, which is accommodated by several rifts, including the Sperchios–North Evia Gulf rift. The extension direction differs slightly (NE–SW to NNE–SSW) within the North Aegean Trough. Specifically, in the North Evia Gulf area, Müller *et al.* (2013) have identified different extensional directions from west to east: 1) NW–SE to NNW–SSE between the Maliakos Gulf and the Central Basin; 2) N–S in North Evia Island and the Central Basin; 3) NNE–SSW around the town of Chalkida and in the southern part of North Evia Island (see Figure 2 for locations).

Based on land-based brittle deformation analysis, the North Evia region has experienced three tectonic phases (Mercier *et al.*, 1979, 1987) since the early formation of the Sperchios–North Evia Gulf rift in Pliocene times. First, from the early Pliocene to the early Pleistocene, an extensional regime characterised by NNE–SSW stress resulted in the formation of large normal faults striking N110 to N120 in the Reginio Basin and North Evia Gulf rift (Figure 2). Second, a short compressional period has been attributed to the early to middle Pleistocene (Philip, 1976; Roussoyannis-Tsiambaou, 1984). The occurrence of this compressional episode is not fully accepted, as several authors have not found evidence of compressional structures (Ganas, 1997; Galanakis *et al.*, 1998; Roberts and Ganas, 2000). Last, from the middle Pleistocene to the present day, the region is dominated by major NNW–SSE to N–S extensional deformation (Mercier *et al.*, 1979, 1987) that has been confirmed by GPS data, as mentioned above (*e.g.* Müller et al., 2013).

The Reginio Basin, also called the Lokris Basin, is a narrow, uplifted and emerged basin between the Kallidromon and Knimis ranges (Figure 2). Its sedimentary infill is mainly composed of lacustrine and fluvial sediments (Dermitzakis and Papanikolaou, 1981; Kranis, 2007) that have been deposited since Late Miocene or Early Pliocene (Celet and Delcourt, 1960; Symeonidis, 1974; Lemeille, 1977; Ioakim, 1986). The Reginio Basin is bordered by two of the major normal fault systems within the North Evia domain: the Kallidromon–Atalanti–Martino (KFS and AMFS) and the Kamena Vourla–Arkitsa (KVAFS) fault systems (Figure 2), which resulted from a broadly N–S direction of extension (Kranis, 2007).

In the western extension of the North Evia Gulf, the Sperchios Basin is considered an asymmetrical graben, mainly controlled by the north-dipping normal faults of the Sperchios–Ipati Fault Zone (Eliet and Gawthorpe, 1995; Kilias *et al.*, 2008, SIFZ in Figure 2). This basin was initiated during the Pliocene and is mainly filled with Pleistocene and Holocene sedimentary deposits (Apostolopoulos, 2005; Pechlivanidou *et al.*, 2014, 2018). Based on resistivity and gravity data, Apostolopoulos (2005) have observed the complex geometry of the top-basement surface below the Neogene deposits, with a strong longitudinal partitioning along the rift and the several small sub-basins.

There are several faults on North Evia Island; the NE–SW-directed Kechriae and Prokopi–Pilion normal Fault Zones (KEFZ and PPFZ, Palyvos *et al.*, 2006, Figure 2) along the edge of the Nileas Depression (Palyvos *et al.*, 2006) are of particular interest. These faults likely control the subsidence of the Nileas Depression and the corresponding relative uplift of the Ksiron and Kandili topographic highs (Palyvos *et al.*, 2006). The current seismicity of the North Evia region highlights the present activity along these fault zones, as well as several other fault segments.

The North Evia Gulf has been subdivided into three sub-basins by Sakellariou *et al.* (2007): the Western Basin (WB), the Central Basin, and the South-Eastern Basin, here called the Eastern Basin (EB, Figure 2). The Western Basin is oriented E–W and displays more pronounced subsidence in the south than in the north. It is a shallow bathymetric area (~100 m maximum water depth) filled by deltaic sediments originating from Mount Knimis and Reginio Basin (Figure 2). The northern boundary of the Central Basin is very steep and is controlled by a major fault system: the Aedipsos–Politika Fault System (APFS, Figure 2). Although the strike differs greatly between the NW–SE fault segments and the almost E–W fault segments near Aedipsos, these fault segments are treated as part of the same fault system because they share the same characteristics (relative age, throw, Holocene slip rate) and they form the northern boundary of the rift. The southern boundary of the Central Basin also seems to be controlled by normal faults (Sakellariou *et al.*, 2007). This deformation zone is studied in much greater detail in the present study. The final sub-basin, the Eastern Basin, similar to the Western Basin, is also shallow (~100 m maximum water depth) and is cross-cut by the NW–SE-striking, seismologically active Melouna Fault Zone (Ganas *et al.*, 2016, MFZ in Figure 2). Van Andel and Perissoratis (2006) and Sakellariou *et al.* (2007) have focussed on the distribution of the Holocene sedimentary unit in these three sub-basins. This unit

corresponds to the Upper Sequence (US) and was dated as Holocene from gravity and box core sampling and analysis by Sakellariou *et al.* (2007).

3. Data and methods

In order to improve our understanding of the geology of the North Evia region, an offshore geophysics approach based on the acquisition of very high-resolution seismic data (Sparker) was used. The datasets were acquired during the WATER 1 and 2 surveys aboard R/V *Téthys II* in 2017 and 2021. The study area included the North Evia Gulf, the Maliakos Gulf, the Lichades Zone, the Oreoi and Artemision Channels, and the Skopelos Basin (Figure 3). Our seismic profiles overlap a previous single-channel airgun seismic dataset (Sakellariou *et al.*, 2007) in the North Evia Gulf (Figure 3).

Previously investigated by Van Andel and Perissoratis (2006) and Sakellariou *et al.* (2007), the North Evia Gulf has been described through high-resolution Sparker (500–1000 Joules, single-channel) and 10 in^3 airgun (single-channel) seismic profiles. The WATER surveys acquired ~1800 km of very high-resolution Sparker seismic profiles (50–300 Joules, single-channel) using a SIG Sparker and a high-resolution single-channel streamer as the receiver. The data acquisition trace intervals range from 333 ms in very shallow areas to 3333 ms in the deepest areas surveyed. We chose to apply a band-pass filter with corner frequencies of 50, 100, 500, and 1000 Hz to eliminate noise. The expected vertical and horizontal resolutions were between 1 and 4 m. The dense network of the Sparker profiles enables accurate interpretations and correlations with previous studies and provides data from non- or poorly documented areas, such as the Maliakos Gulf, the Oreoi and Artemision Channels, and the Skopelos Basin (Figure 3).

The WATER data was acquired at various water depths (Figure 3). The shallowest parts were located around the volcanic Lichades Islands, in the bay of Livanates, and in the Oreoi Channel, where some profiles have been recorded with only a few metres of water (Figures 2 and 3). On these profiles, the first sea-bottom multiple, which is a seismic artefact, appears rapidly. The deepest parts of the survey area were located in the Central Basin of the North Evia Gulf and the Skopelos Basin (Figures 2 and 3).

Numerous correlations between the airgun and the Sparker datasets are possible and allow tectonic and sedimentary interpretations through the entire North Evia Gulf in particular, in the Upper Sequence, which is considered to be from the Holocene (Van Andel and Perissoratis, 2006; Sakellariou *et al.*, 2007). This Upper Sequence enables the estimation

of the relative age of deformations. All the seismic interpretation was achieved following the seismic stratigraphy approach developed by Mitchum *et al.* (1977). The Upper Sequence has been recognised for its erosive basis accompanied by onlaps and downlaps.

We also used published bathymetric and topographic data from EMODnet and SRTM30 datasets, respectively (Farr *et al.*, 2007, Figure 2), to create a Geographic Information System (GIS) database. Bathymetry data can help to map significant morphological expressions of faults identified by seismic data if they appear on the sea floor. In order to discuss the activity of faults and the nature of the deformation within the North Evia region, we exploited several earthquake and focal mechanism databases (United States Geological Survey Latest Earthquakes, Aristotle University of Thessaloniki, Global Project Centroid Moment Tensor, Ekström *et al.*, 2012, International Seismological Centre, Storchak *et al.*, 2013; Di Giacomo *et al.*, 2018, and microseismicity studies from Kiratzi, 2002). The ages of the main geological units have been added to the GIS database from the 1:50000 geological maps of IGME (Institute of Geology and Mineral Exploration, Marinos *et al.*, 1957, 1963, 1967; Papastamatiou *et al.*, 1960, 1962; Maratos *et al.*, 1965, 1967; Tataris *et al.*, 1970; Katsikatsos *et al.*, 1978a, 1978b, 1980, 1981; Parginos *et al.*, 2007). We chose to map the Quaternary, Neogene, and Jurassic (Pelagonian) sedimentary units and the ophiolite units separately (Figure 4). It is, therefore, possible to observe the different Neogene sedimentary basins, the Jurassic Pelagonian basement rocks, and the ophiolite nappes. This allows us to discuss the location of deformation and the possible role of inherited structures.

In this study, we considered three categories of fault in terms of timing in order to precisely place recent and active deformation in North Evia: 1) the faults affecting the bathymetry, 2) the faults shifting horizons from the Upper Sequence but not the sea floor, and 3) the faults sealed by the base of the Upper Sequence or older horizons. To determine the vertical offsets along the faults, we measured the time offsets on seismic lines, and we depth-converted the obtained values using seismic velocities from 1600 to 2000 $m \cdot s^{-1}$ according to the young ages of the observed sedimentary units and the velocity ranges provided by Press (1966), Mavko *et al.* (1998), and Stewart (2011) for siliciclastic sediments. A mean velocity of 1800 $m \cdot s^{-1}$ was used to estimate the throws in the sediments. We used a velocity of 1500 $m \cdot s^{-1}$ in seawater to estimate the sea floor offsets. The measures of offsets along the normal offshore faults identified from the seismic analysis were performed within the youngest seismic units affected by deformation. In the case of faults affecting the bathymetry, the offsets were deduced from the observed shift in the bathymetry. In the shallower areas, where

only the Upper Sequence was observed, the measured offsets are minimal. Therefore, they may be underestimates. Consequently, some faults now considered minor, with activity during the Holocene or older, could have played a more important role during previous deformation phases. All the seismic profiles (Sakellariou *et al.*, 2007 and WATER surveys, Figure 3) were interpreted using the IHS Kingdom Suite software. Then, the interpretations were integrated into a GIS database built using QGIS (QGIS.org, 2023). We complemented our offshore investigations with fieldwork on North Evia Island, the Reginio Basin, and the southern coasts of the North Evia Gulf. The seismic profiles presented in this paper are vertically exaggerated to show the angular relationship between the seismic units more clearly. Because of this vertical exaggeration, the faults appear vertical or with a very high dip angle. To determine the displacement, we worked with non-exaggerated profiles, leading to the characterisation of the real dip angle. Several faults were distinguished as major faults when they affected the bathymetry and showed offsets larger than 50 m. The offshore structural analysis allowed us to update the structural map of the North Evia Gulf, provide new insights into the Oreoi and Artemision Channels and Skopelos Basin, and compile the onshore faults to present the major deformation zones within the whole North Evia region, onshore and offshore (Figure 4). Four specific zones are detailed in the following sections: the Lichades Zone, North Evia Gulf, Oreoi Channel, and Skopelos Basin.

4. Results

4.1. Seismic interpretation

4.1.1. Identification of the seismic units

This study presents new interpretations and insights into the fault networks (Figure 4) within the whole North Evia region, especially in the North Evia Gulf. We present the approach we used based on analysing seismic facies (Table 1) and identifying major fault zones both offshore and onshore.

Using seismic profile analysis, three major seismic units were distinguished from top to bottom: the Upper Sequence, Unit A (UA), and Unit B (UB). They are defined by different seismic facies and terminations of reflectors (toplaps, downlaps, and onlaps, Table 1). Based on the studies of Van Andel and Perissoratis (2006) and Sakellariou *et al.* (2007), the Upper Sequence has been identified and characterised in the very high-resolution WATER survey profiles. This unit is considered to be post-glacial Holocene marine sedimentary fill (Van Andel and Perissoratis, 2006; Sakellariou *et al.*, 2007). It allows us to determine the relative

ages of faults and associated deformations. The Upper Sequence constitutes three parallel to sub-parallel and high-frequency seismic facies: SF1, with strong continuity and moderate amplitudes; SF2, with high continuity and high amplitudes; and SF3, with moderate continuity and low amplitudes (Table 1).

The boundary between the Upper Sequence and Unit A is an erosion surface (B1, Table 1) marked by toplaps in Unit A and overlapped by onlaps within the Upper Sequence. Unit A mainly consists of parallel to sub-parallel reflector geometries (SF2 and SF4) and, within a certain area, chaotic facies covered by undulated reflectors (SF5). All these seismic facies show high frequencies and amplitudes. Unit B comprises four seismic facies with low or low to moderate amplitudes and different degrees of continuity (Table 1). The Unit A–Unit B boundary (B2, Table 1) is characterised by seismic facies amplitude changes. Some profiles located in the Oreoi Channel show erosional truncation between Units A and B.

4.1.2. Identification of the offshore faults

More than 1500 fault offsets have been identified from the 452 seismic profiles available in the North Evia region (airgun and Sparker data). From our interpretations, 140 faults have been individually identified by correlating the observed fault offsets to seismic lines. They have been reported on a GIS to propose the new structural map presented in this study (Figure 4). In order to supplement the existing fault datasets in Greece (Ganas *et al.*, 2013), we present the details of a selection of 46 main faults (Table 2) within the North Evia region (Figure 5). We also provide the corresponding KML file in the Appendix.

These faults are representative of the deformation of their respective areas. The maximum youngest throw has been measured in the youngest unit affected by the fault. The relative age has been estimated according to three different markers: 1) offset in the bathymetry (post-US), 2) activity during the Holocene Upper Sequence, but the sea floor is not affected (Syn-US), and 3) no deformation during the Holocene (Pre-US). We consider the faults that offset the Upper Sequence to be active. This leads to considering the Pre-US faults as inactive. The Holocene slip rates were calculated from offsets of the base of the Upper Sequence, and the knowledge that the Holocene started 11.7 kyr ago (Cohen *et al.*, 2013). As the Upper Sequence is not identifiable in the Skopelos Basin, we could not determine Holocene slip rates for the faults in this part of the study area.

4.2. Deformation in the North Evia region

4.2.1. The Lichades Zone

The Lichades Zone extends from the Maliakos Gulf to the Lichades Peninsula (Li) and from the Oreoi Channel to the coasts of Central Greece (Figures 4 and 6). This area defines the transition zone between the Sperchios Basin and the North Evia Gulf, constituting the Sperchios–North Evia Gulf rift. The Lichades Zone is characterised by ~500,000-year-old calc-alkaline volcanism belonging to the Aegean volcanic arc (Pe-piper and Piper, 1989; Innocenti *et al.*, 2010). From seismic data, we interpreted the chaotic seismic facies covered by strongly undulated reflectors at the top as lava flows from the Lichades volcanic structures (Figure 7).

The Lichades Zone (Figure 6) is mainly controlled by north and south-dipping normal faults, directed E–W, with small offsets generally not exceeding ~12 m (15 ms TWTT, Figures 7 and 8). A different deformation pattern with folded high-amplitude reflectors was observed close to the volcanic islands. This area forms a horst-like shoal, the northern margin of which is a well-marked north-dipping normal fault (Figure 7). The deformation along other faults becomes younger towards the south, and the offsets are larger than in the north (Figure 8). The southern faults dip northwards while the northern ones dip southward. Thus, this area shows a small graben (Figures 6 and 8).

The northern part of the WAT17_124 profile is characterised by at least one anticline and a major north-dipping normal fault with a ~6 m (~8 ms TWTT) offset at the sea floor (Figure 7). This normal fault, called the Oreoi Fault (OrF), corresponds to the Li10 fault (Table 2). We consider this fault active, as shown by the throws within the Holocene (US), the offset, and the bathymetry. Thus, we estimated a minimum Holocene slip rate of 0.77 mm/yr. The anticline axis was not apparent in another seismic profile, so it is not possible to correlate it and determine its direction.

The southernmost fault in Figure 8 is listed as Li3 in Table 2. This normal fault displays a maximum throw at the base of the Holocene of ~5.4 m (6 ms TWTT). This limit is below the first multiple of the sea floor (M); therefore, this interpretation of the seismic reflector is uncertain. As illustrated in Figures 7 and 8, the Upper Sequence depocentre is located in the southern part of the Lichades Zone, close to the shoreline, with a thickness reaching ~40 m (50 ms TWTT). The southwards thickening of Upper Sequence deposits

cannot be verified as controlled by an offshore fault. It could be controlled by the Molos Fault or another segment of the inland Kamena Vourla–Arkitsa Fault System (Figure 6).

4.2.2. The North Evia Gulf

The North Evia Gulf rift is located between North Evia Island and Central Greece (Figure 9). This gulf can be divided into three sub-basins based on morphological and structural data, as mentioned above. Two main fault systems control the deformation within the North Evia Gulf: the offshore Aedipsos–Politika Fault System (Figure 8), which borders the southern coast of North Evia Island, and the onshore Atalanti–Martino Fault System, which runs from Atalanti to Larymna (Figures 4 and 9).

The Aedipsos–Politika Fault System dips southwards with a significant change in direction from E–W between Aedipsos and Mount Telethrion to NW–SE between Mount Telethrion and Limni (Figure 9, Sakellariou *et al.*, 2007; this study). This fault system coincides with an important bathymetric scarp on the northern margin of the North Evia Gulf. According to some authors (*e.g.* Sakellariou *et al.*, 2007; Evelpidou *et al.*, 2012), the Aedipsos–Politika Fault System could extend to the southern coast of Mount Kandili and continue inland across the Politika plain (Politika Fault/PoF, Figure 9). However, the available seismic data do not give a precise location for the Aedipsos–Politika Fault System south of Limni. Thus, we represent this southern propagation with a dashed line in Figure 9.

4.2.2.1. The Western Basin (WB)

The deformation within the Western Basin is restricted to several faults east of the basin at the boundary with the Central Basin. These faults define the Western Fault Zone (Figure 8). This zone forms a complex graben characterised by fault segments with various directions, mainly E–W and NNE–SSW (Figures 9 and 10). The highest fault offsets occur along the faults that dip south and south-east (Figures 9 and 10). This graben separates two structural domains that show different seismic facies and deformation styles. The northern domain, referred to here as the Aedipsos Platform, can be divided into three zones by considering the significant variations in reflector geometries (Figure 10). From south to north, the first zone shows low-dipping reflectors with an overall anticline shape cut by normal faults (1, Figure 10). The second zone appears more intensely folded and highly disrupted by faults that are difficult to interpret because of the lack of reliable seismic markers (2, Figure 10). Finally, the third zone is characterised by high-angle north-dipping reflectors, which progressively decrease in dip to the north, towards the coast of North Evia Island (3, Figure

10). Thus, the Aedipsos Platform corresponds to an intensely deformed area where the faults and the folds cannot be correlated due to the lack of seismic profiles.

The southern region of the Western Basin shows several normal faults with small offsets and one major normal fault located close to the southern boundary of the basin (Figure 10). The latter, labelled as WB4 in Table 2 and Figure 5, dips northwards and offsets the base of the Holocene by ~12.6 m (~14 ms TWTT). Considering that, we estimated a minimum Holocene slip rate of 1.08 mm/yr. In the hanging wall of these normal faults, the Upper Sequence presents large thicknesses (~30 ms TWTT, ~27 m thick) with a southward open fan shape. Beneath the Upper Sequence, the offset of the Unit A sequence appears much larger than the offset of the Upper Sequence, although it is impossible to correlate the reflectors of Unit A and Unit B on either side of the fault. It is noteworthy that, in the hanging wall, Unit A and Unit B are folded, whereas those of the Upper Sequence are sub-horizontal. The origin of these folds remains unclear, although the normal fault is very clear.

4.2.2.2. The Central Basin (CB)

The Central Basin Fault System (CBFS) extends from the east of the Arkitsa Fault (Ar) to the north of the Malesina Peninsula (Figure 9). Mainly directed WNW–ESE, this fault system shows large offsets (~50–70 m) along the southern slope of the deep basin (Figures 11 and 12). The major fault segments of the Central Basin Fault System are referred to as CB2 and CB6 in Table 2 and Figure 5. These faults present a minimum Holocene slip rate of 5.38 mm/yr. In the north, the Central Basin is bordered by the faults of the Aedipsos–Politika Fault System (Figures 9 and 11). One of these faults, labelled CB1 (Table 2), displays an offset of at least ~55 m (74 ms) in the bathymetry and a minimum estimated Holocene throw of 7.08 mm/yr.

On its western side, the reflectors of Unit A are south-dipping in the platform area but become slightly north-dipping towards the northern edge of the platform area (Figure 11). In the Central Basin, the platform area is located in the south (Figures 11 and 12). On the eastern side of the Central Basin Fault System, between the Malesina Peninsula and Limni, the reflectors are sub-horizontal on the platform and slightly south-dipping in the slope area (Figure 12). Unit B shows sub-horizontal reflectors from east to west on the platform that become south-dipping towards the slope (Figures 11 and 12). The reflectors in the deep basin display a northward fan shape, open towards one of the faults of the Aedipsos–Politika Fault System (Figure 11).

The north-dipping faults between the platform and the Central Basin are the major faults of the Central Basin Fault System (Figure 9). The other segments of the Central Basin Fault System, located towards the south of the profile, individualise a few small grabens (km-scale in length) with smaller offsets than those to the south (5–30 ms TWTT, Figures 9, 11, and 12), which do not affect the sea floor.

4.2.2.3. The Eastern Basin (EB)

The Eastern Basin (Figure 9) presents major deformation along the NW–SE-striking Melouna Fault Zone (MFZ, Sakellariou *et al.*, 2007). The most important segment with the largest offsets dips south-westwards. The westernmost segment of the Melouna Fault Zone (EB1 in Table 2 and Figure 5) affects the bathymetry and displays a maximum Holocene throw of approximately 6.3 m (7 ms TWTT). Thus, the minimum Holocene vertical slip rate is estimated at 0.54 mm/yr. The Melouna Fault Zone is marked by significant seismic activity with strike-slip focal mechanisms suggesting left-lateral displacements (Ganas *et al.*, 2016 and compilations realised in this study). The Melouna Fault Zone separates the Eastern Basin into two sub-basins. The northern sub-basin (Kandili) is characterised by a northward thickening of the Upper Sequence and the older units, corresponding to Unit A and Unit B (Figure 13). The Eastern Basin shows a singular seismic unit composed of undulated reflectors (URU, Figure 13) observed only in this area. Units A and B could not be correlated from the northern to the eastern sub-basins. Nevertheless, the same strong differences in seismic facies are present between the strong-amplitude facies beneath the Upper Sequence and the weak-amplitude facies beneath the undulated reflectors, compared with those between Units A and B in the Western and Central Basins (Figure 13). On both sides of the undulated reflectors, these units are hypothetically referred to as Unit A and Unit B (UA? and UB? in Figure 13).

Thus, three main directions of normal faults are present in the North Evia Gulf: NW–SE, WNW–ESE, and E–W (Figures 4 and 9). The WNW–ESE orientation is the most common, and some faults with this direction show bathymetric offsets locally exceeding ~55.5 m (70 ms TWTT).

4.2.3. The Oreoi Channel

The Oreoi-Artemision Channel is a 60-km-long narrow straight (3 to 10 km wide) that connects the North Evia Gulf to the Skopelos Basin (Figure 4). From the available data, the Oreoi Channel (OC, Figure 4) does not contain very intense deformation. A few normal faults

are observed across the channel axis (Figures 4 and 14). At least one of these faults affects the Holocene Upper Sequence and coincides with a small bathymetric scarp (OC3, Table 2, Figures 5 and 14, offset of ~2.25 m, 3 ms TWTT). The observed offsets reach about 22.5 m (25 ms TWTT) at depth, at the limit between sequences interpreted as Unit A and Unit B (UA? and UB? in Figure 14).

4.2.4. The new Skiathos Basin

The Skiathos Basin is a major depocentre at the NE end of the Artemision Channel, newly discovered from the WATER seismic dataset. Indeed, prior to this study, no marine data except bathymetry existed, and no significant depression was observed in the bathymetric data because the basin is almost filled by recent sediments (Figure 15). Our seismic interpretations revealed several major structural elements in this key area between Skiathos Island and the NE–SW-oriented Oreoi–Artemision Channel.

The Skiathos Basin is separated from the deep-water Skopelos Basin (Figure 15) by a partly buried structural ridge characterised by chaotic seismic facies (Figures 16 and 17). We name this ridge the "Evia–Skiathos Ridge", and we interpret this acoustic basement high as most probably composed of the Mesozoic basement. Other basement asperities, with similar chaotic seismic facies, are completely buried in this area, including the opposite border of the Skiathos Basin (Figures 16 and 17).

Several seismic sequences were deposited between these basement ridges, forming three individual depocentres. By the time of the deposition of one of the most recent sequences (S6), these small depocentres were connected to form a singular Skiathos Basin (Figure 16), leading to the burial of most of the ridges. The S6 sequence belongs to the distal part of the sixth clinoform sequence of a large Quaternary system prograding north-eastwards out of the Artemision Channel (Caroir, 2022). The uppermost sediments are correlated with the Holocene Upper Sequence (US, Figures 15 and 16). Within the main depocentre, the basin reaches a thickness of at least 225 m (250 ms TWTT, down to the sea-bottom multiple).

Further north, the main depocentre slightly widens, and the smaller one has less lateral continuity, although they still exist between the uneven basement ridges (Figure 17). This main depocentre also displays some normal faults, that are dipping westward (Figure 16) or eastward (Figure 17). These dipping variations occur on short distances (few kilometres) along strike. (Figure 15). The older sedimentary units also show some flexures and very heterogeneous distribution. These small deep depocentres, flexed sediments, and opposing

fault dips, together with the rapid along-strike variation in structural geometries, evoke a strike-slip corridor (*e.g.* Barnes and Audru 1999). The main faults identified in the basin are NE–SW-striking with apparent normal offsets (Figures 15, 17 and 17). The main NW-dipping fault (Figure 16), referenced as Skib1 (Table 2 and Figure 5), predates the S6 unit and shows an offset of approximately 13.5 m (15 ms TWTT) in the pre-S6 series. The main SE-dipping fault (Figure 17), referenced as Skib2 (Table 2 and Figure 5), mainly offsets the pre-S6 series but also shows a moderate offset at the base of this S6 unit (approx. 3.6 m, *i.e.* 4 ms TWTT). Although these normal faults show opposite dips, they belong to the same faulted corridor that was active during the Quaternary but not since the beginning of the Holocene, as they are clearly buried by the Holocene Upper Sequence.

4.2.5. The Skopelos Basin

The Skopelos Basin is located between North Evia and Skopelos Island (Figures 3 and 15). This triangular basin constitutes the deepest area of the North Evia region (~1050 m depth). Its south-eastern boundary is formed by several seamounts oriented roughly NE–SW, with depths ranging from 100 to 400 m (Figure 15). These seamounts are located near a very steep slope to the deep basin (Figure 4). From our seismic data interpretations, the south-eastern boundary is mainly controlled by a major fault striking NE–SW that we have named the South Skopelos Fault (SSF, Figures 15 and 18). This fault, running along a 13-km-long scarp, is NW-dipping and shows a major vertical offset of up to several hundred metres (Figure 18). Sakellariou and Tsampouraki-Kraounaki (2019) have also reported major faults in this region with WNW–ESE direction and secondary faults trending NNE–SSW.

4.3. Analysis of brittle deformation in the North Evia Island

Field data were acquired on North Evia Island in September 2019 (Figure 19) to (1) document possible correlations between faulting on land and major offshore fault segments and (2) to constrain the kinematics of recent faults from brittle deformation analysis in Neogene to Quaternary sediments. Among the several strike-slip faults identified from sub-horizontal striations, some were reliable indicators of dextral (blue faults on stereonets, Figure 19) or sinistral movement (red faults on stereonets, Figure 19). Our field observations also reveal a large NE–SW-striking dextral strike-slip fault east of Limni (6, Figure 19) and a large NW–SE-striking sinistral strike-slip fault near the Artemision Channel (1, Figure 19). The latter has the same direction as a nearby normal fault, extracted from the National Observatory of Athens (NOA) fault database (Figure 19, Ganas *et al.*, 2013). In the northernmost part of Evia, other sets of faults also showing this NW–SE direction are normal,

with dip-slip slickensides (stereonet 2, Figure 19) consistent with the NOA fault mentioned above (*i.e.* Ganas *et al.*, 2013).

The eastern coast of North Evia also shows sets of conjugate strike-slip faults (*e.g.* stereonet 4, Figure 19) that can be interpreted as the result of either NNE–SSW extension or ENE–WSW compression. The occurrence of numerous normal faults (stereonet 3, Figure 19), with decametric to metric-scale offsets, giving evidence for N–S to NNE–SSW extension, suggests that the sets of strike-slip faults are also associated with that extensional deformation. Along the south coast of North Evia, near Limni, a similar structural pattern can be observed with c. NE–SW-directed dextral strike-slip faults and c. NW–SE-directed sinistral strike-slip faults (stereonet 8, Figure 19). These fault orientations are compatible with the N–S direction of extension inferred from sets of normal faults (*e.g.* stereonet 7, Figure 19).

5. Discussion

The seismic profile analysis highlights three main seismic units: the Upper Sequence, Unit A, and Unit B. Previous studies have interpreted Upper Sequence as Holocene post-glacial filling (Van Andel and Perissoratis, 2006; Sakellariou *et al.*, 2007). Units A and B are older than the Upper Sequence, but we cannot specify their ages. Consequently, the fault kinematic interpretations are restricted to the Holocene, and the slip rates are estimated on the offsets of the Upper Sequence base. This method could underestimate the slip rates if the fault initiated during the Holocene (Table 2). Despite that, high slip rates were measured in the rift basins: 1.15 mm/yr in the Lichades Zone, 1.69 mm/yr in the Western Basin and 5–7 mm/yr in the Central Basin.

5.1. Discussion of the main faulted regions

- ***The Oreoi Fault (OrF)***

In the Lichades Zone, a north-dipping normal fault was identified from seismic data, which significantly offsets the bathymetry (Li10 in Table 2 and Figure 5, OrF in Figure 7). This fault trace appears in the western extension of the NE–SW-striking Oreoi normal fault along the north-western border of the Lichades Peninsula that has been mentioned in previous studies (Galanakis *et al.*, 1998; Palyvos *et al.*, 2006; Kilias *et al.*, 2008). Thus, this fault seems to be one of the main active structures within the Lichades Zone, playing a major role in the present-day deformation and the development of the Oreoi Channel.

- ***The Western Fault Zone (WFZ)***

The Western Fault Zone, located in the Western Basin, consists of two main normal faults with opposite dip directions (Figure 10). They both affect the seafloor with significant offsets (~7 m). This configuration displays a well-expressed linear trough that represents an active graben. Nevertheless, this obvious linear structure does not show significant lateral extension. The major fault bordering the graben to the north (Figure 10; WB7 in Table 2 and Figure 5) is the most continuous and is relatively easy to correlate as it separates two very different structural domains: the Western Basin and the Aedipsos Platform (Figure 10). For this reason, we consider the WB7 fault the most important fault within the Western Fault Zone. Its eastern extension remains uncertain, as the fault pattern changes radically to a NE–SW direction (Figure 9). It is unclear whether this change in orientation reflects significant bending of these faults or if the main E–W faults are cross-cut and offset by a secondary set of NE–SW faults. The spacing of the available seismic data in this very complex area does not allow us to fully understand the structural pattern associated with this variation in faulting orientation.

- ***The Central Basin Fault System (CBFS)***

The Central Basin Fault System is dominated by WNW–ESE-striking normal faults (Figure 12), most of which dip to the north (CB2, CB6, CB8, CB9 and CB10 in Table 2 and Figure 5) and show significant offsets in the bathymetry. These are similar to the Kamena Vourla–Arkitsa Fault System in orientation, dipping, and recent activity. Consequently, we interpret the Central Basin Fault System as the offshore propagation of the Kamena Vourla–Arkitsa Fault System. This onshore and offshore fault system corresponds to a major faulted corridor, about 100 km long, most likely representing the main active structure that controls the present-day deformation of the southern side of this segment of the North Evia Gulf rift (*i.e.* Central Basin).

- ***The Aedipsos–Politika Fault System (APFS)***

The northward thickening of the sedimentary units in the Kandili sub-basin suggests the existence of a major syn-sedimentary normal fault at the toe of the Kandili mountains (Figure 9). This fault could not be directly observed from seismic data as it runs along the coastline or at a very shallow depth underwater along the narrow platform. This fault is inferred from the major basement offset between the Kandili mountains and the deep base of the basin, and its existence is supported by recent tectonic activity (Sakellariou *et al.*, 2007; Evelpidou *et al.*, 2012). Our observations of growth strata tilted towards the north also support the existence of a major fault to the north, with tectonic activity coeval with the development

of the North Evia rift. Surprisingly, this NW–SE-directed fault system links westwards to the CB1 fault (Table 2 and Figure 5), which trends E–W, *i.e.* largely oblique to most of the faults in the Aedipsos–Politika Fault System. We still consider this segment part of the same fault system, as it has a similar throw, age, and dip direction. Furthermore, it also corresponds to the northern boundary of the North Evia Gulf rift.

- ***The asymmetry of the Sperchios–North Evia Gulf rift***

The Sperchios–North Evia Gulf rift is usually considered an asymmetric graben (*e.g.*, Goldsworthy and Jackson, 2001; Sakellariou *et al.*, 2007; Caroir, 2022; this study). The subsidence and the deformation in the western part of the Sperchios–North Evia Gulf rift are strongly controlled by the north-dipping faults along the southern margin (Sperchios–Ipati Fault Zone and the fault segments of Molos and Kamena Vourla, Figure 6). The subsidence and the deformation in the Central Basin, and most likely the Eastern Basin, are preferentially controlled by the Aedipsos–Politika Fault System, which is located at the northern margin of the rift. Thus, the western and eastern parts of the Sperchios–North Evia Gulf rift show a strong asymmetry, with a main depocentre to the south and north of the rift axis, respectively. Between these two opposite rift systems (west and east), the Western Basin of the North Evia Gulf appears to be relatively symmetric and forms a transition area between the asymmetric parts. Consequently, we assume that the N070E-striking normal fault of the Oreoi Channel (Oreoi Fault, Figures 4 and 6) plays a significant role in rift development because it delineates the change in the rift geometry. Thus, the results of our marine seismic analysis and compilation of structural data confirm the asymmetric structure of the North Evia Gulf rift and highlight the change in polarity between the Sperchios Basin and the Central Basin.

5.2. The current deformation of the North Evia region

A large number of seismic events (magnitudes from 3 to > 6) have been recorded from the 1970s to the present day (Figure 20-B). Some earthquake swarms indicate a clear E–W direction, and several faults identified in this study can be characterised by seismic activity. Since 550 BCE, many earthquakes have been reported in historical and archaeological records (Figure 20-A). Some were reported in the Maliakos Gulf, the Lichades Zone, south of the Oreoi Channel, and between the Western Basin and Central Basin of the North Evia Gulf (Figure 20-A). The major events have been estimated at Mw 6.4 in 105 CE, close to the Western Fault Zone, Mw 7 in 426 BCE and Mw 6.8 in 551 CE within the Lichades Zone (Figure 20-A). Because the locations and magnitudes are approximate, it is not possible to associate them with a specific fault zone. However, the area of the Maliakos Gulf, the

Lichades Zone, south of the Oreoi Channel, and the Western Fault Zone have historically experienced numerous intense earthquakes. These seismic events indicate significant seismic activity in the complex junction between the Sperchios Basin, the North Evia Gulf, and the Oreoi Channel.

The seismic event maps in Figure 20 highlight the intense activity in the vicinity of the South Skopelos Fault, south of Skiathos Island and near the northern coast of Evia, in the western extension of the North Aegean Trough. The earthquake distribution and the focal mechanism compilation highlight the seismic activity of the study area in the south-western extension of the North Anatolian Fault (Figures 20-B and 21). Moreover, the compilation of fault distributions from previous works, together with geological mapping and our marine survey datasets, allow us to discuss the active deformation inferred from the focal mechanisms. Indeed, the P (pressure) and T (tension) axes issued from these focal mechanisms give us an expression of the active deformation and the strain orientation for most individual major faults (Figure 22).

5.2.1. Right-lateral displacements along major NE–SW faults

Ten major NE–SW-striking faults have been identified in North Evia Island, the Oreoi and Artemision Channels, and the Skopelos Basin (Figures 4, 21, and 22). Inland, the Prokopi–Pilion Fault Zone (Figure 22) is considered an active major normal fault zone participating in the deformation of the Nileas Depression (ND, Figure 21, Palyvos *et al.*, 2006). Some offshore faults (Oreoi Fault and South Skopelos Fault) show significant vertical offsets of the sea floor (~6 m and ~450 m respectively, Table 2).

However, earthquakes characterised by strike-slip focal mechanisms occurred along the Prokopi–Pilion Fault Zone, along offshore faults in the Oreoi and Artemision Channels, and in the northernmost parts of North Evia Island. Our field observations revealed NE–SW-directed strike-slip faults with well-marked slickensides east of Limni (6, Figure 19). Assuming that the earthquakes described by strike-slip focal mechanisms took place along these NE–SW-striking faults, they show right-lateral displacements (Figures 21 and 22). Strike-slip reactivations along former normal faults have been recently observed from a new Mw 5 earthquake (3rd November 2023) along the Prokopi–Pilion Fault Zone, with dextral motions along NE-SW direction. Accordingly, we consider that most of these NE–SW faults were originally normal faults with significant vertical offsets before acting as dextral strike-slip faults at least at present-day.

5.2.2. Left-lateral displacements along major faults

The NW–SE-directed faults from the Aedipsos–Politika Fault System and the Melouna Fault Zone constitute the northern border of the North Evia Gulf rift following the initiation of rifting during the Pliocene (Jackson, 1999; Goldsworthy and Jackson, 2001; Kranis, 2007; Sakellariou *et al.*, 2007). These major faults present relatively large cumulative vertical offsets. Currently, they show several strike-slip focal mechanisms, which means that their kinematics changed during the rifting. Our field observations on North Evia Island found additional strike-slip faults, striking NW–SE with clear horizontal slickensides (1 and 8, Figure 19). Assuming that the earthquakes characterised by the strike-slip focal mechanisms occurred along these NW–SE fault systems, they must correspond to left-lateral displacements (Figures 21 and 22). Thus, we assume that the early normal faults (Aedipsos–Politika Fault System and Melouna Fault Zone) formed during the rifting have recently been reactivated and currently show significant left-lateral displacements.

The southern margin of the North Evia Gulf rift is delineated by the Kallidromon–Atalanti–Martino and the Kamena Vourla–Arkitsa Fault Systems. These fault systems are NW–SE- and WNW–ESE-directed, respectively, and present high cumulative vertical offsets. Field observations from some of these faults show oblique slip directions with a left-lateral component (Figures 21 and 22, Ganas *et al.*, 1998; Kokkalas *et al.*, 2007; Kranis, 2007; Jones *et al.*, 2009).

Further north, south-east of Alonissos Island (Figures 21 and 22), another major NW–SE-directed fault system is characterised by active left-lateral strike-slip displacements, as shown by seismological data (Ganas *et al.*, 2005; Papanikolaou *et al.*, 2019; data compilation realised in this study). This fault system develops at the termination of the southern branch of the North Anatolian Fault, which borders the Skyros Basin (Papanikolaou *et al.*, 2019).

Most of these active strike-slip corridors are located along faults that dip ~60° to 75° and display a large cumulative vertical offset (*e.g.* ~1000 m for the Arkitsa Fault, Jackson and McKenzie, 1999; Kokkalas *et al.*, 2007; Jones *et al.*, 2009), leading to their interpretation as former normal faults. The oblique slip evidenced in the field with slickensides on exposed fault mirrors also supports such relative chronology. In our study, we assume that most of these faults were created during the early extensive episodes associated with the initial development of the rift. Several paleomagnetic studies (Kissel *et al.*, 1989; Bradley *et al.*, 2013) have demonstrated the significance of rotations in this region, which had to be

considered to reconstruct the deformation history of the region and understand the present complex fault pattern.

5.3. Possible role of the North Anatolian Fault

Currently, the North Evia region does not show any clear fault segments sharing characteristics with the North Anatolian Fault (NAF). The ~20-km-long South Skopelos Fault (Figures 15 and 18) might be a good candidate for a fault segment extending the North Anatolian Fault to the SW. It is the main fault bordering the Skopelos Basin, trends NE–SW, and is responsible for a major scarp in the bathymetry (>500 m). Nevertheless, this fault line is not significantly impacted by recent seismicity, and no strike-slip focal mechanisms can be attributed to it. Some historical earthquakes have occurred in this area, particularly on the northern part of this fault. However, due to the approximate locations, assigning them to this specific fault with much confidence is challenging.

Furthermore, our study highlights some new NE–SW-directed fault lines, as well as a narrow basement structure (the Evia–Skiathos Ridge), and also some NE–SW-directed faults along the Oreoi–Artemision Channel. We show evidence for an unknown basin, the "Skiathos Basin" (section 4.2.4.), at the NE end of the Artemision Channel, characterised by a NE–SW-trending deformation pattern that could be related to strike-slip deformation (Figures 15, 16, and 17). Moreover, some earthquakes in this deformation zone showed strike-slip focal mechanisms compatible with dextral displacements in the NE–SW direction. All these observations suggest that some dextral strike-slip deformation could develop along the Oreoi–Artemision Channel in the SW extension of the North Aegean Trough and the North Anatolian Fault (Figures 21 and 22). Thus, we propose that some dextral deformations along former normal faults could be influenced by transferred strain from the North Anatolian Fault.

6. Conclusions

Based on the interpretation of very high-resolution Sparker and high-resolution airgun seismic datasets, the present study provides detailed documentation of the offshore fault systems and a structural map of the North Evia Gulf and its vicinity. These new insights accurately illustrate the recent and active fault patterns within nearby young rifts located immediately southwest of the North Anatolian Fault and the associated North Aegean Trough, in the plate boundary zone between the Anatolia–Aegean and Eurasian plates.

Our results outline the structural complexity of the young North Evia Gulf rift (~3.6 Ma old), where normal fault systems with different directions coexist and remain active. Seismic data analysis shows kilometre-scale cumulative vertical offsets of the major NW–SE faults bordering the rift, whereas recent left-lateral movements along some of these faults are documented by earthquake focal mechanisms. A second generation of large normal faults, striking WNW–ESE, also presents large vertical offsets, and most of their lateral onshore extensions display oblique slip directions with a left-lateral component (*e.g.* Arkitsa Fault). This study details the eastern offshore propagation of this well-known coastal fault system, including the Arkitsa Fault.

We show that the most recent fault pattern, related to the third generation of normal faulting, is E–W-directed. These large normal faults delineate the western part of the rift system, including the Sperchios Basin and the Maliakos Gulf. Some E–W-trending faults have also developed along the rift axis in the Western Basin and in the Lichades Zone. These faults reflect the present-day N–S extension, also indicated by focal mechanisms and geodetic data. Compiling seismicity data and focal mechanisms revealed active left-lateral displacements along some of the major NW–SE striking faults, such as the Aedipsos–Politika Fault System and the Melouna Fault Zone. Such reactivation of the former NW–SE-directed normal faults is compatible with the present-day N-S extensional deformation. In the south-western extension of the NE–SW-striking North Anatolian Fault, several faults sharing the same orientation have been identified. The seismicity along these structures, and associated focal mechanisms, show active right-lateral displacements that are also compatible with the general N–S extensional deformation over the whole area.

Our seismic datasets also revealed and described a new basin depocentre, the Skiathos Basin, in the south-western extension of the North Anatolian Fault and the North Aegean Trough. The Skiathos Basin developed in the axis of the Oreoi–Artemision Channel and is bounded to the east from the Aegean Sea by a partially buried narrow basement ridge extending between North Evia and Skiathos Island. Moreover, our dataset allowed us to significantly improve the tectonic framework of the Skopelos Basin, which is bordered to the east by a major NE–SW-striking normal fault parallel to the SW branches of the North Anatolian Fault.

Some additional data, such as deeper seismic profiles and drilling, are necessary to fully understand the origin and development of the Skiathos Basin, with its complicated sedimentary record and deformation patterns. This basin and its surroundings represent a key

area in understanding the whole region, including the processes and timing of the southwest propagation of the North Anatolian Fault. Despite the remaining work to be undertaken, this study provides significant structural data to improve our knowledge of the development of the North Evia region and our understanding of this rather diffuse boundary between Eurasia, the Aegean Sea and the North Anatolian Fault. These new insights into the tectonic framework of the whole North Evia area can improve both seismic hazard assessment and future strain models.

Acknowledgements

The authors thank the UMR-8187 LOG (Laboratoire d'Océanologie et de Géosciences) for financial and logistic support; in particular, we thank Monique Gentric for her great efficiency. This work was supported by the Tellus program of CNRS-INSU ("SYSTER" and "post-campagne à la mer") for field work and processing of marine data. We also thank IFREMER and the research team "TIMES" of the LOG for providing funding to organise both cruises (WATER1, 2017 and WATER2, 2021). The Sparker equipment was funded by the European Union (ERDF), the French State, the French Region Hauts-de-France, and Ifremer in the framework of the project CPER MARCO 2015–2021. The authors warmly acknowledge the crew of R/V *Téthys II* for technical support. We also warmly thank Athanasios Ganas and Kristóf Porkolab for their highly constructive reviews that greatly improved an earlier version of the manuscript and Gideon Rosenbaum for his very constructive comments and editorial assistance.

References

Angiolini, L., Dragonetti, L., Muttoni, G., Nicora, A., 1992. Trias stratigraphy in the island of Hydra (Greece).

Apostolopoulos, G., 2005. Geophysical studies relating to the tectonic structure, geothermal fields and geomorphological evolution of the Sperchios River Valley, Central Greece 14.

Armijo, R., Meyer, B., King, G. C. P., Rigo, A., Papanastassiou, D., 1996. Quaternary evolution of the Corinth rift and its implication for the late Cenozoic evolution of the Aegean. Geophysical Journal International, 126, 11-53.

Armijo, R., Meyer, B., Hubert, A., Barka, A., 1999. Westward propagation of the North Anatolian fault into the northern Aegean: Timing and kinematics. Geology, 27, 267-270.

Baud, A., Jenny, C., Papanikolaou, D., Sideris, Ch., Stampfli, G., 1991. New observations on permian stratigraphy in Greece and geodynamic interpretation.

Barnes, P.M., Audru, J.-C., 1999. Recognition of active strike-slip faulting from high-resolution marine seismic reflection profiles: Eastern Marlborough fault system, New Zealand. GSA Bulletin, 111 (4), 538-559.

Beccaluva L., Coltorti M., Saccani E., Siena F., 2005. Magma generation and crustal accretion as evidenced by supra-subduction ophiolites of the Albanide-hellenide SubPelagonian zone. Isl Arc, 14, 551–563.

Beniest, A., Brun, J.P., Gorini, C., Crombez, V., Deschamps, R., Hamon, Y., Smit, J., 2016. Interaction between trench retreat and Anatolian escape as recorded by neogene basins in the northern Aegean Sea. Marine and Petroleum Geology, 77, 30–42. https://doi.org/10.1016/j.marpetgeo.2016.05.011.

Bernard, P., Lyon-Caen, H., Briole, P., Deschamps, A., Boudin, F., Makropoulos, K., Papadimitriou, P., Lemeille, F., Patau, G., Billiris, H., Paradissis, D., Papazissi, K., Castarède, H., Charade, O., Nercessian, A., Avallone, A., Pacchiani, F., Zahradnik, J., Sacks, S., Linde, A., 2006. Seismicity, deformation and seismic hazard in the western rift of Corinth: new insights from the Corinth rift laboratory (Crl). Tectonophysics, 426, 7–30.

Bonneau, M., 1984. Correlation of the Hellenide nappes in the south-east Aegean and their tectonic reconstruction. Geological Society London Special Publications, 17, 517–527. https://doi.org/10.1144/GSL.SP.1984.017.01.38.

Bradley, K.E., Vassilakis, E., Hosa, A., Weiss, B.P., 2013. Segmentation of the Hellenides recorded by Pliocene initiation of clockwise block rotation in Central Greece. Earth and Planetary Science Letters, 362, 6–19. https://doi.org/10.1016/j.epsl.2012.11.043.

Brun, J.-P., Faccenna, C., 2008. Exhumation of high-pressure rocks driven by slab rollback. Earth and Planetary Science Letters, 272, 1–7. https://doi.org/10.1016/j.epsl.2008.02.038.

Brun, J.-P., Sokoutis, D., 2010. 45 m.y. of Aegean crust and mantle flow driven by trench retreat. Geology, 38, 815-818. http://dx.doi.org/10.1130/G30950.1.

Brun, J.-P., Faccenna, C., Gueydan, F., Sokoutis, D., Philippon, M., Kydonakis, K., Gorini, C., 2016. The two-stage Aegean extension, from localized to distributed, a result of slab rollback acceleration. Can. J. Earth Sci., 53, 1142-1157.

Brunn, J.H., Argyriadis, I., Ricou, L.E., Poisson, A., Marcoux, J., de Graciansky, P.C., 1976. Elements majeurs de liaison entre Taurides et Hellenides. Bulletin de la Société Géologique de France S7-XVIII, 481–497. https://doi.org/10.2113/gssgfbull.S7-XVIII.2.481

Burchfiel, B.C., Nakov, R., Dumurdzanov, N., Papanikolaou, D., Tzankov, T., Serafimovski, T., King, R.W., Kotzev, V., Todosov, A., Nurce, B., 2008. Evolution and dynamics of the Cenozoic tectonics of the South Balkan extensional system. Geosphere, 4, 919-938. https://doi.org/10.1130/GES00169.1.

Burg, J.-P., 2012. Rhodope: From Mesozoic convergence to Cenozoic extension. Review of petro-structural data in the geochronological frame. J. Virt. Ex, 42, 1-44. https://doi.org/10.3809/jvirtex.2011.00270.

Caroir, F., 2022. Analyse structural du domaine Nord Eubée : rifting plio-quaternaire et décrochements actifs dans le prolongement occidental de la Faille Nord-Anatolienne (Projet WATER). Thèse de doctorat, Université de Lille, France, 209p.

Celet, P., Delcourt, A., 1960. Les terrains néogènes de Locride (Grèce orientale moyenne), leur situation géologique et leur âge. Annales de la Société Géologique du Nord, 80, 125-132.

Chousianitis, K., Ganas, A., Gianniou, M., 2013. Kinematic interpretation of present-day crustal deformation in central Greece from continuous GPS measurements. Journal of Geodynamics, 71, 1-13. 10.1016/j.jog.2013.06.004.

Clarke, P.J., Davies, R.R., England, P.C., Parsons, B., Billiris, H., Paradissis, D., Veis, G., Cross, P.A., Denys, P.H., Ashkenazi, V., Bingley, R., Kahle, H.-G., Muller, M.-V., Briole, P., 1998. Crustal strain in central Greece from repeated GPS measurements in the interval 1989-1997. Geophys. J. Int., 135, 195–214. https://doi.org/10.1046/j.1365-246X.1998.00633.x.

Clément, B., 1983. Evolution géodynamique d'un secteur des Hellénides internes : l'Attique-Béotie (Grèce continentale). Thèse de l'Université de Lille, 521p., Lille.

Cohen, K.M., Finney, S.C., Gibbard, P.L., Fan, J.X., 2013 (updated) The ICS International Chronostratigraphic Chart. Episodes 36 : 199-204.

Collier, R.E.L., Dart, C.J., 1991. Neogene to quaternary rifting, sedimentation and uplift in the Corinth basin, Greece. J; Geol. Soc. Lond., 148, 1049–1065.

Dercourt J., 1970. L'expansion océanique actuelle et fossile : ses implications géotectoniques. Bull. Soc. Geol. France, 12, 261–317.

Dercourt, J., Zonenshain, L.P., Ricou, L.-E., Kazmin, V.G., Le Pichon, X., Knipper, A.L., Grandjacquet, C., Sbortshikov, I.M., Geyssant, J., Lepvrier, C., Pechersky, D.H., Boulin, J., Sibuet, J.-C., Savostin, L.A., Sorokhtin, O., Westphal, M., Bazhenov, M.L., Lauer, J.P., Biju-Duval, B., 1986. Geological evolution of the tethys belt from the Atlantic to the pamirs since the LIAS. Tectonophysics, 123, 241–315. https://doi.org/10.1016/0040-1951(86)90199-X.

Dermitzakis, M.D., Papanikolaou, D.J., 1981. Paleogeography and Geodynamics of the Aegean region during the Neogene. Proc. of 1st Intern. Congress on Mediterranean Neogene, Athens, 27 September – 2 October 1979, 245-289.

Dewey, J.F., Sengör, A.M.C., 1979. Aegean and surrounding regions: complex multiplate and continuum tectonics in a convergent zone. Geol. Soc. Am. Bull., 90, 84-92.

Di Giacomo, D., Engdahl, E.R., Storchak, D.A., 2018. The ISC-GEM Earthquake Catalogue (1904–2014): status after the Extension Project, Earth Syst. Sci. Data, 10, 1877-1899, doi: 10.5194/essd-10-1877-2018.

Dilek Y., Furnes H., Shallo M., 2008. Geochemistry of the Jurassic Mirdita Ophiolite (Albania) and the MORB to SSZ evolution of a marginal basin oceanic crust. Lithos., 100, 174–209.

Drakos, A.G., Stiros, S.C., Kiratzi, A.A., 2001. Fault parameters of the 1980 (M_w 6.5) Volos, Central Greece, Earthquake from Inversion of Repeated Leveling Data. Bulletin of the Seismological Society of America, 91, 1673-1684.

Ekström, G., Nettles, M., Dziewonski, A.M., 2012. The global CMT project 2004-2010: Centroid-moment tensors for 13,017 earthquakes, Phys. Earth Planet. Inter., 200-201, 1-9. Doi: 10.1016/j.pepi.2012.04.002.

Eliet, P.P., Gawthorpe, R.L., 1995. Drainage development and sediment supply within rifts, examples from the Sperchios basin, central Greece. Journal of the Geological Society, London, 152, 883-893.

EMODnet Bathymetry Consortium (2020): EMODnet Digital Bathymetry (DTM).

Evelpidou, N., Vassilopoulos, A., Pirazzoli, P.A., 2012. Holocene emergence in Euboea island (Greece). Marine Geology, 295-298, 14-19. 10.1016/j.margeo.2011.11.010.

Farr, T.G., Rosen, P.A., Caro, E., Crippen, R., Duren, R., Hensley, S., Kobrick, M., Paller, M., Rodriguez, E., Roth, L., Seal, D., Shaffer, S., Shimada, J., Umland, J., Werner, M., Oskin, M., Burbank, D., Alsdorf, D., 2007. The Shuttle Radar Topography Mission. Reviews of Geophysics, 45, RG2004, doi:10.1029/2005RG000183.

Faucher, A., Gueydan, F., Jolivet, M., Alsaif, M., Célérier, B., 2021. Dextral Strike-Slip and Normal Faulting During Middle Miocene Back-Arc Extension and Westward Anatolia Extrusion in Central Greece. Tectonics, 40, e2020TC006615. https://doi.org/10.1029/2020TC006615.

Faure, M., Bonneau, M., 1988. Données nouvelles sur l'extension néogène de l'Egée : la déformation ductile du granite miocène de Mykonos (Cyclades, Grèce). Comptes rendus de l'Académie des sciences. Série 2, Mécanique, Physique, Chimie, Sciences de l'univers, Sciences de la Terre, 307 (13),1553-1559.

Ferentinos, G., Georgiou, N., Christodoulou, D., Geraga, M., Papatheodorou, G., 2018. Propagation and termination of a strike slip fault in an extensional domain: The westward growth of the North Anatolian Fault into the Aegean Sea. Tectonophysics, 745, 183-195. Doi.org/10.1016/j.tecto.2018.08.003.

Ferrière J., 1972. Sur l'importance des déplacements tangentiels en Othrys centrale au NE d'Anavra (Grèce). C. R. Acad. Sci. Paris, 274**,** 174-176.

Ferrière J., 1974. Étude géologique d'un secteur des zones helléniques internes sub-pélagoniennes (massif de l'Othrys, Grèce orientale). Importance et signification de la période orogénique anté-Crétacé supérieur. Bull. Soc. Géol. France, XVI (5), 543–562.

Ferrière J., 1976. Sur la signification des séries du massif de l'Othrys (Grèce continentale) : la zone isopique Maliaque. Ann. Soc. Géol. Nord, 96 (2), 121–134.

Ferriere J., Stais A., 1994. Un ou des bassin(s) téthysien(s) vardarien(s). 7th Congress of the Geological Society, Thessalonique, Greece, p. 91–103.

Ferrière J., Stais A., 1995. Nouvelle interprétation de la suture téthysienne vardarienne d'après l'analyse des séries de Péonias (Vardar oriental, Hellenides internes). Bull. Soc. Geol. France, 166, 327–339.

Ferrière, J., Chanier, F., Ditbanjong, P., 2012. The Hellenic ophiolites: eastward or westward obduction of the Maliac Ocean, a discussion. Int J Earth Sci (Geol Rundsch), 101, 1559–1580. https://doi.org/10.1007/s00531-012-0797-9.

Ferrière, J., Baumgartner, P.O., Chanier, F., 2016. The Maliac Ocean: the origin of the Tethyan Hellenic ophiolites. Int. J., Earth Sci., 10.1007/s00531-016-1303-6.

Flotté, N., Sorel, D., Müller, C., Tensi, J., 2005. Along strike changes in the structural evolution over a brittle detahcment fault: example of the Pleistocene Corinth-Patras rift (Greece). Tectonophysics, 403, 77–94.

Floyd, M.A., Billiris, H., Paradissis, D., Veis, G., Avallone, A., Briole, P., McClusky, S., Nocquet, J.-M., Palamartchouk, K., Parsons, B., England, P.C., 2010. A new velocity field for Greece: Implications for the kinematics and dynamics of the Aegean. J. Geophys. Res., 115, B10403. https://doi.org/10.1029/2009JB007040.

Ford, M., Williams, E.A., Malatre, F., Popescu, S.P., 2007. Stratigraphic architecture, sedimentology and structure of the Vouraikos Gilbert-type delta, gulf of Corinth, Greece. I.A.S. Spec. Publ., 38, 49–90.

Galanakis, D., Pavlides, S., Mountrakis, D., 1998. Recent brittle tectonics in Almyros–Pagasitikos, Maliakos, N. Euboea and Pilion. Bulletin of the Geological Society of Greece, 23, 263–273 (in Greek).

Ganas, A., 1997. Fault segmentation and seismic hazard assessment in the Gulf of Evia rift, central Greece. PhD Thesis, University of Reading, United Kingdom, 426p.

Ganas, A., Roberts, G.P., Memou, T., 1998. Segment boundaries, the 1894 ruptures and strain patterns along the Atalanti Fault, Central Greece. Journal of Geodynamics, 26, 461–486. https://doi.org/10.1016/S0264-3707(97)00066-5.

Ganas, A., Drakatos, D., Pavlides, S.B., Stavrakakis, G.N., Ziazia, M., Sokos, E., Karastathis, V.K., 2005. The 2001 Mw=6.4 Skyros earthquake, conjugate strike-slip faulting and spatial variation in stress within the central Aegean Sea. Journal of Geodynamics, 39, 61-77.

Ganas, A., Parsons, T., 2009. Three-dimensional model of Hellenic Arc deformation and origin of the Cretan uplift. Journal of Geophysical Research, 114, B06404, doi:10.1029/2008JB005599.

Ganas, A., Oikonomou, I.A., Tsimi, C., 2013. NOAfaults: a digital database for active faults in Greece. Bulletin of the Geological Society of Greece, 47, 518-530. https://doi.org/10.12681/bgsg.11079.

Ganas, A., Mouzakiotis, E., Moshou, A., Karastathis, V., 2016. Left-lateral shear inside the North Gulf of Evia Rift, Central Greece, evidenced by relocated earthquake sequences and moment tensor inversion. Tectonophysics, 682, 237-248. https://doi.org/10.1016/j.tecto.2016.05.031.

Gautier, P., Brun, J.-P., 1994. Crustal-scale geometry and kinematics of late-orogenic extension in the central Aegean (Cyclades and Evia Island). Tectonophysics, 238, 399–424. https://doi.org/10.1016/0040-1951(94)90066-3.

Goldsworthy, M., Jackson, J., 2001. Migration of activity within normal fault systems: examples from the Quaternary of mainland Greece. Journal of Structural Geology, 23, 489–506.

Goldsworthy, M., Jackson, J., Haines, J., 2002. The continuity of active fault systems in Greece. Geophysical Journal International, 148, 596–618.

Grasemann, B., Schneider, D.A., Stöckli, D.F., Iglseder, C., 2012. Miocene bivergent crustal extension in the Aegean: Evidence from the western Cyclades (Greece). Lithosphere, 4, 23–39. https://doi.org/10.1130/L164.1.

Guernet, C., 1971. Contribution à l'étude géologique de l'Eubée et des régions voisines. Thesis, Université Paris VI, 395 pp.

Hatzfeld, D., Ziazia, M., Kementzetzidou, D., Hatzidimitriou, P., Panagiotopoulos, D., Makropoulos, K., Papadimitriou, P., Deschamps A., 1999. Microseismicity and focal mechanisms at the western termination of the North Anatolian Fault and their implications for continental tectonics. Geophysical Journal International, 137, 891-908.

Hejl, E., Bernroider, M., Parlak, O., Weingartner, H., 2010. Fissiontrack thermochronology, vertical kinematics, and tectonic development along the western extension of the North Anatolian Fault zone, J. Geophys. Res., 115, B10407, doi:10.1029/2010JB007402.

Hollenstein, Ch., Müller, M.D., Geiger, A., Kahle, H.-G., 2008. Crustal motion and deformation in Greece from a decade of GPS measurements, 1993-2003. Tectonophysics, 449, 17-40.

Hubert-Ferrari, A., Armijo, R., King, G., Meyer, B., Barka, A., 2002. Morphology, displacement, and slip rates along the North Anatolian Fault, Turkey. J. Geophys. Res. 107, ETG 9-1-ETG 9-33. https://doi.org/10.1029/2001JB000393.

Hubert-Ferrari, A., King, G., Manighetti, I., Armijo, R., Meyer, B., Tapponnier, P., 2003. Long-term elasticity in the continental lithosphere; modelling the Aden Ridge and the Anatolian extrusion process. Geophysical Journal International, 153, 111-132.

Hynes A., Nisbet E.G., Smith A.G., Welland M.J.P. and Rex D.C., 1972. Spreading and emplacement ages of some ophiolites in the Othris region (eastern central Greece). Zeitschrift der Deutschen Geologischen Gesellschaft., 123, 455-468.

Innocenti, F., Agostini, S., Doglioni, C., Manetti, P., Tonarini, S., 2010. Geodynamic evolution of the Aegean: constraints from the Plio-Pleistocene volcanism of the Volos – Evia Area. Journal of the Geological Society, London, 167, 475-489.

International Seismological Centre (2021), On-line Bulletin, https://doi.org/10.31905/D808B830.

Ioakim Ch., 1986. Palynological. – Stratigraphical study of the L3 borehole in Agnandi, Lokris. IGME Unpubl. Report, Athens, 4p (in Greek)

Jackson, J., 1999. Fault death: a perspective from actively deforming regions. Journal of Structural Geology, 21, 1003–1010. https://doi.org/10.1016/S0191-8141(99)00013-9.

Jackson, J., McKenzie, D., 1999. A hectare of fresh striations on the Arkitsa Fault, central Greece. Journal of Structural Geology, 21, 1-6.

Jolivet, L., Daniel, J.M., Truffert, C., Goffé, B., 1994. Exhumation of deep crustal metamorphic rocks and crustal extension in arc and back-arc regions. Lithos, 33, 3–30. https://doi.org/10.1016/0024-4937(94)90051-5.

Jolivet, L., 2003. Subduction tectonics and exhumation of high-pressure metamorphic rocks in the Mediterranean orogens. American Journal of Science, 303, 353–409. https://doi.org/10.2475/ajs.303.5.353.

Jolivet, L., Rimmelé, G., Oberhänsli, R., Goffé, B., Candan, O., 2004. Correlation of syn-orogenic tectonic and metamorphic events in the Cyclades, the Lycian nappes and the Menderes massif. Geodynamic implications. Bulletin de la Société Géologique de France, 175, 217–238. https://doi.org/10.2113/175.3.217.

Jolivet, L., Brun, J.-P., 2010. Cenozoic geodynamic evolution of the Aegean. Int. J. Earth Sci., 99, 109-138.

Jolivet, L., Labrousse, L., Agard, P., Lacombre, O., Bailly, V., Lecomte, E., Mouthereau, F., Mehl, C., 2010. Rifting and shallow-dipping detahcments, clues from the Corinth Rift and the Aegean. Tectonophysics, 483, 287–304.

Jolivet, L., Faccenna, C., Huet, B., Labrousse, L., Le Pourhiet, L., Lacombe, O., Lecomte, E., Burov, E., Denèle, Y., Brun, J.-P., Philippon, M., Paul, A., Salaün, G., Karabulut, H., Piromallo, C., Monié, P., Gueydan, F., Okay, A.I., Oberhänsli, R., Pourteau, A., Augier, R., Gadenne, L., Driussi, O., 2013. Aegean tectonics: Strain localisation, slab tearing and trench retreat. Tectonophysics, 597–598, 1–33. https://doi.org/10.1016/j.tecto.2012.06.011.

Jones, R., Kokkalas, S., McCaffrey, K., 2009. Quantitative analysis and visualization of non-planar fault surfaces using terrestrial laser scanning (LIDAR) – The Arkitsa fault, central Greece, as a case study, Geosphere, 5, 465–482, doi:10.1130/GES00216.1.

Katsikatsos, G., Koukis, G., Mettos, A., Albantakis, N., Machairas, G., 1978. Geological map of Larymna at 1:50 000 scale, published by IGME.

Katsikatsos, G., Mettos, A., Vidakis, M., Tsaïla-Monopolis, ST., Skourtsi-Koroneu, V., Ioakim, C., Chorianopoulou, P., Papazeti, E., Hadjicostanti-Tsalahouri, I., Georgiou-Nikolaidou, A., Giftopoulou, CH., 1978b. Geological map of Istiaia at 1:50 000 scale, published by IGME.

Katsikatsos G., Kounis, G., Fytikas, M., Mettos, A., Vidakis, M., Tsaïla-Monopolis, ST., Bornovas, J., 1980. Geological map of Limni at 1:50 000 scale, published by IGME.

Katsikatsos, G., Koukis, G., Fytikas, M., Anastopoulos, J., Kanaris, J., Tsaïla-Monopolis, ST., Bornobas, J., 1981. Geological map of Psachna at 1:50 000 scale, published by IGME.

Ketin, I., 1948. Son on yılda Türkiye'de vukua gelen büyük deprem- lerin tektonik ve mekanik neticeleri hakkında. Bulletin of the Geological Society of Turkey, 13.

Kilias, A.A., Tranos, M.D., Papadimitriou, E.E., Karakostas, V.G., 2008. The recent crustal deformation of the Hellenic orogen in Central Greece; the Kremasta and Sperchios Fault Systems and their relationship with the adjacent large structural features. Zdgg, 159, 533–547. https://doi.org/10.1127/1860-1804/2008/0159-0533.

Kilias, A., Frisch, W., Avgerinas, A., Dunkl I., Falalakis, G., Gawlick, H.J., 2010. Alpine architecture and kinematics of deformation of the northern Pelagonian nappe pile in the Hellenides. Austrian Journal of Earth Sciences, 103, 4-28.

Kilias, A., 2021. The Hellenides: A Multiphase Deformed Orogenic Belt, its Structural Architecture, Kinematics and Geotectonics Setting during the Alpine Orogeny: Compression vs Extension the Dynamic Peer for the Orogen Making. A Synthesis. Journal of Geology and Geoscience, 5, 1-57.

Kiratzi, A.A., 2002. Stress tensor inversions along the westernmost North Anatolian Fault Zone and its continuation into the North Aegean Sea. Geophysical Journal International 151, 360–376. https://doi.org/10.1046/j.1365-246X.2002.01753.x.

Kissel, C., Laj, C., Poisson, A., Simeakis, K., 1989. A pattern of block rotations in central Aegea, in Paleomagnetic Rotations and Continental Deformation, edited by C. Kissel and C. Laj, pp. 115–129, Kluwer Acad., Dordrecht, Netherlands, doi:10.1007/978-94-009-0869-7_8.

Kissel, C., Laj, C., Poisson A., Görür, N., 2003. Paleomagntic reconstruction of the Cenozoic evolution of the Eastern Mediterranean. Tectonophysics, 362, 199–217.

Kokkalas, S., Jones, R.R., McCaffrey, K.J.W., Clegg, P., 2007. Quantitative fault analysis at Arkitsa, Central Greece, using terrestrial laser-scanning ("LIDAR"). Bulletin of the Geological Society of Greece, 37, 1-14.

Kondopoulou, D., Caputo, R., 1997. Palaeomagnetic evidence for non-rotational deformation along the Nea Anchialos Fault System, Central Greece. Annali di Geofisica, 40, 1-9.

Kranis, H., 2007. Neotectonic Basin Evolution In Central-Eastern Mainland Greece: An Overview. Bulletin of the Geological Society of Greece, 37, 1-14. https://doi.org/10.12681/bgsg.16621.

Kreemer, C., Chamot-Rooke, N., Le Pichon, X., 2004. Constraints on the evolution and vertical coherency of deformation in the Northern Aegean from a comparison of geodetic, geologic and seismological data. Earth Planet. Sci. Lett., 225, 329-346.

Leeder, M.R., Mack, G.H., Brasier, A.T., Parrish, P.R., McIntosh, W.C., Andrews, J.E., Duermeijer, C.E., 2008. Late-Pliocene timing of Corinth (Greece) rift-margin fault migration. Earth Planet. Sci. Lett., 274, 132–141.

Leeder, M.R., Mark, D.F., Gawthrope, R.L., Kranis, H., Loveless, S., Pedentchouk, N., Skourtsos, E., Turner, J., Andrews, J.E., Stamatakis, M., 2012. A "Great Deepening": Chronology of rift climax, Corinth Rift, Greece. Geology, 40, 999–10002. doi:10.1130/G33360.1.

Lemeille F., 1977. Études néotectoniques en Grèce centrale nord-orientale (Eubée centrale, Attique, Béotie, Locride) et dans les Sporades du Nord. Thèse, Univ. Paris XI.

Le Pichon, X., Angelier, J., 1979. The Hellenic Arc and trench system: A key to the neotectonic evolution of the Eastern Mediterranean area. Tectonophysics, 60, 1-42.

Le Pichon, X., Angelier, J., 1981. The Aegean Sea. Phil. Trans. R. Soc. Lond. A., 300, 357–372. https://doi.org/10.1098/rsta.1981.0069.

Le Pichon, X., Kreemer, C., 2010. The Miocene-to-Present Kinematic Evolution of the Eastern Mediterranean and Middle East and Its Implications for Dynamics. Annu. Rev. Earth Planet. Sci., 38, 323–351. https://doi.org/10.1146/annurev-earth-040809-152419.

Le Pichon, X., İmren, C., Rangin, C., Şengör, A.M.C., Siyako, M., 2014. The South Marmara Fault. Int. J. Earth Sci. (Geol Rundsch), 103, 219–231. https://doi.org/10.1007/s00531-013-0950-0.

Le Pichon, X., Şengör, A.M.C., Kende, J., İmren, C., Henry, P., Grall, C., Karabulut, H., 2016. Propagation of a strike-slip plate boundary within an extensional environment: the westward propagation of the North Anatolian Fault. Can. J. Earth Sci., 53, 1416–1439. https://doi.org/10.1139/cjes-2015-0129.

Lips, A.L.W., White, S.H., Wijbrans, J.R., 1998. $^{40}Ar/^{39}Ar$ laserprobe direct dating of discrete deformational events: a continuous record of early Alpine tectonics in the Pelagonian Zone, NW Aegean area, Greece. Tectonophysics, 298, 133-153.

Makris, J., Papoulia, J., Yegorova, T., 2013. A 3-D density model of Greece constrained by gravity and seismic data. Geophysical Journal International, 194, 1–17. https://doi.org/10.1093/gji/ggt059.

Maratos, G., Rigopoulos, K., Athanassiou, A., Zachos, K., 1965. Geological map of Atalanti at 1:50 000 scale, published by IGME.

Maratos, G., Rigopoulos, K., Athanassiou, A., Zachos, K., 1967. Geological map of Elatia at 1:50 000 scale, published by IGME.

Marinos, G., Anastopoulos, J., Maratos, G., Melidonis, N., Andronopoulos, B., Zachos, K., 1957. Geological map of Myli at 1:50 000 scale, published by IGME.

Marinos, G., Anastopoulos, J., Maratos, G., Melidonis, N., Andronopoulos, B., Zachos, K., 1963. Geological map of Stylis at 1:50 000 scale, published by IGME.

Marinos, G., Anastopoulos, J., Maratos, G., Melidonis, N., Andronopoulos, B., Papastamatiou I., Tataris, Ath., Vetoulis, D., Bornovas, G., Katsikatsos, G., Maragoudhakis, N., Lalekhos, N., Zachos, K., 1967. Geological map of Lamia at 1:50 000 scale, published by IGME.

Mavko, G., Mukerji, T., Dvorkin, J., 1998. The Rock Physics Handbook. Cambridge University Press, Cambridge.

McClusky, S., Balassanian, S., Barka, A., Demir, C., Ergintav, S., Georgiev, I., Gurkan, O., Hamburger, M., Hurst, K., Kahle, H., Kastens, K., Kekelidze, G., King, R., Kotzev, V., Lenk, O., Mahmoud, S., Mishin, A., Nadariya, M., Ouzounis, A., Paradissis, D., Peter, Y., Prilepin, M., Reilinger, R., Sanli, I., Seeger, H., Tealeb, A., Toksöz, M.N., Veis, G., 2000. Global Positioning System constraints on plate kinematics and dynamics in the eastern Mediterranean and Caucasus. J. Geophys. Res., 105, 5695–5719. https://doi.org/10.1029/1999JB900351.

McKenzie, D.P., 1970. Plate Tectonics of the Mediterranean Region. Nature, 226, 239–243. https://doi.org/10.1038/226239a0.

McKenzie, D., 1972. Active Tectonics of the Mediterranean Region. Geophysical Journal International, 30, 109–185. https://doi.org/10.1111/j.1365-246X.1972.tb02351.x.

McKenzie, D., 1978. Active tectonics of the Alpine--Himalayan belt: the Aegean Sea and surrounding regions. Geophysical Journal International, 55, 217–254. https://doi.org/10.1111/j.1365-246X.1978.tb04759.x.

McKenzie, D., Jackson, J., 1983. The relationship between strain rates, crustal thickening, palaeomagnetism, finite strain and fault movements within a deforming zone. Earth and Planetary Science Letters, 65, 182–202. https://doi.org/10.1016/0012-821X(83)90198-X.

Menant, A., Jolivet, L., Vrielynck, B., 2016. Kinematic reconstructions and magmatic evolution illuminating crustal and mantle dynamics of the eastern Mediterranean regions since the late Cretaceous. Tectonophysics, 675, 103-140.

Mercier, J.L., Delibassis, N., Gauthier, A., Jarrige, J.L., Lemeille, F., Philip, H., Sebrier, M., Sorel, D., 1979. La néotectonique de l'arc égéen. Revue de géologie dynamique et de géographie physique, 21, 67-92.

Mercier, J.-L., 1981. Extensional-compressional tectonics associated with the Aegean Arc: Comparison with the Andean Cordillera of South Peru-North Bolivia, Philos. Trans. R. Soc. London Ser. A, 300, 337- 355.

Mercier, J.L., Sorel, D., Simeakis, K., 1987. Changes in the state of stress in the overriding plate of a subduction zone: The Aegean Arc from the Pliocene to the Present.

Mitchum, R.M., Jr., Vail, P.R., Thompson, S., 1977. Seismic Stratigraphy and Global Changes of Sea Level: Part 2. The Depositional Sequence as a Basic Unit for Stratigraphic Analysis. In: Payton, C. E. (ed.), Seismic Stratigraphy – Applications to Hydrocarbon Exploration. American Association of Petroleum Geologists Memoir, 26, 53–62.

Moretti, I., Sakellariou, D., Lykousis, V., Micarelli, L., 2003. The Gulf of Corinth: an active half graben? J. Geodyn., 36, 323–340.

Mountrakis, D., 1987. The Pelagonian Zone in Greece. A polyphaser deformed fragment of the Cimmerian Continent and its role in the geotectonic evolution of the Mediterranean. J. Geol., 94, 335–347.

Mouslopoulou, V., Sudhaus, H., Konstantinou, K. I., Begg, J., Saltogianni, V., Mannel, B., Andinisari, R., Oncken, O., 2022. A deeper look into the 2021 Tyrnavos Earthquake Sequence (TES) reveals coseismic breaching of an unrecognized large-scale fault relay zone in continental Greece. Tectonics, 41, e2022TC007453. https://doi.org/10.1029/2022TC007453.

Müller, M.D., Geiger, A., Kahle, H.-G., Veis, G., Billiris, H., Paradissis, D., Felekis, S., 2013. Velocity and deformation fields in the North Aegean domain, Greece, and implications for fault kinematics, derived from GPS data 1993–2009 16. Tectonophysics, 597-598, 34-49.

Nixon, C.W., McNeill, L.C., Bull, J.M., Bell, R.E., Gawthorpe, R.L., Henstock, T.J., Christodoulou, D., Ford, M., Taylor, B., Sakellariou, D., Ferentinos, G., Papatheodorou, G., Leeder, M.R., Collier, R.E.L. Goodliffe, A.M., Sachpazi, M., Kranis, H., 2016. Rapid spatiotemporal variations in rift structure during development of the Corinth Rift, central Greece. Tectonics, 35, 1225–1248.

Novikova, T., Mouzakiotis, E., Karastathis, V.K., 2017. Magnitude Assessment for the Historical Earthquake Based on Strong-Motion Simulation and Liquefaction Analysis: Case of the 1894 Atalanti Earthquake, Greece. Bulletin of the Seismological Society of America, 107, 418–432. https://doi.org/10.1785/0120150267.

Palyvos, N., Bantekas, I., Kranis, H., 2006. Transverse fault zones of subtle geomorphic signature in northern Evia island (central Greece extensional province): An introduction to the Quaternary Nileas graben. Geomorphology, 76, 363–374. https://doi.org/10.1016/j.geomorph.2005.12.002.

Papanikolaou, D., Alexandri, M., Nomikou, P., 2006. Active faulting in the north Aegean basin, in Dilek, Y., and Pavlides, S., eds., Postcollisional tectonics and magmatism in the Mediterranean region and Asia. Geological Society of America Special Paper, 409, 189-209.

Papanikolaou, D., Nomikou, P., Papanikolaou, I., Lampridou, D., Rousakis, G., Alexandri, M., 2019. Active tectonics and seismic hazard in Skyros Basin, North Aegean Sea, Greece. Marine Geology, 407, 94–110. https://doi.org/10.1016/j.margeo.2018.10.001.

Papastamatiou, I., Tataris, Ath., Vetoulis, D., Bornovas, G., Christodoulou, G., Katsikatsos, G., Zachos, K., 1960. Geological map of Amfissa at 1:50 000 scale, published by IGME.

Papastamatiou, I., Tataris, Ath., Vetoulis, D., Katsikatsos, G., Lalechos, N., Elefteriou, A., Zachos, K., 1962. Geological map of Amfiklia at 1:50 000 scale, published by IGME.

Papoulia, J., Makris, J., Drakopoulou, V., 2006. Local seismic array observations at north Evoikos, central Greece, delineate crustal deformation between the North Aegean Trough and Corinthiakos Rift. Tectonophysics, 423, 97-106.

Parginos, D., Mavrides, A., Bornovas, I., Mettos, A., Katsikatsos, G., Koukis, G., Christodoulou, G., Tsaila-Monopolis, ST., Skourtsi-Koroneou, V., Ioakim CH., Dimou-Honiotaki, E., Kanaki-Mavridou, F., Tsalahouri IR., Foundou, CHR., Georgiou, A., Vacalopoulou EUC., 2007. Geological map of Chalkida at 1:50 000 scale, published by IGME.

Pechlivanidou, S., Vouvalidis, K., Lovlie, R., Nesje, A., Albanakis, K., Pennos, C., Syrides, G., Cowie, P. and Gawthorpe, R., 2014. A multi-proxy approach to reconstructing sedimentary environments from the Sperchios Delta, Greece. Holocene, 24, 1825–1839.

Pechlivanidou, S., Cowie, P., Hannisdal, B., Whittaker, A., Gawthorpe, R., Pennos, C., Riiser, O., 2018. Source-to-sink analysis in an active extensional setting: Holocene erosion and deposition in the Sperchios rift, Central Greece. Basin Research, 30, 522-543.

Pe-Piper, G., Panagos, A.G., 1989. Geochemical characteristics of the triassic volcanic rocks of Evia: petrogenetic and tectonic implications. Ofioliti, 33-50.

Pe-Piper, G., Piper, D.J.W., 1989. Spatial and temporal variation in Late Cenozoic back-arc volcanic rocks, Aegean Sea region. Tectonophysics, 169, 113-134.

Permanent Regional Seismological Network operated by the Aristotle University of Thessaloniki, doi:10.7914/SN/HT (Accessed March 09, 2021).

Pérouse. E, Chamot-Rooke, N., Rabaute, A., Briole, P., Jouanne, F., Georgiev, I., Dimitrov, D., 2012. Bridging onshore and offshore present-day kinematics of central and eastern Mediterranean: Implications for crustal dynamics and mantle flow. Geochemistry, Geophysics, Geosystems, 13, Q09013, doi:10.1029/2012GC004289.

Philip, H., 1976. Un épisode de déformation en compression à la base de Quaternaire en Grèce Centrale (Locride et Eubée nord-occidentale), Bull. Soc. Géol. France, 18, 287-292.

Porkoláb, K., Willingshofer, E., Sokoutis, D., Creton, D., Kostopoulos, D., Wijbrans, J., 2019. Cretaceous-Paleogene tectonics of the Pelagonian zone: inferences from Skopelos Island (Greece). Tectonics, 38(6), 1946-1973. https://doi.org/10.1029/2018tc005331.

Porkoláb, K., Willingshofer, E., Sokoutis, D., Wijbrans, J., 2020. Strain localization during burial and exhumation of the continental upper crust: a case study from the Northern Sporades (Pelagonian thrust, Greece). Glob. Planet. Chang., 194, 103292.

Porkoláb, K., Willingshofer, E., Sokoutis, D., Békési, E., Beekman, F., 2023. Post-5 Ma rock deformation on Alonnisos (Greece) constrains the propagation of the North Anatolian Fault. Tectonophysics, 846, 229654. https://doi.org/10.1016/j.tecto.2022.229654.

Press, F., 1966. Seismic velocities. In: Clark Jr., S.P. (Ed.), Handbook of Physical Constants, Revised Edition. Geological Society of America Memoir, 97, 97-173.

QGIS.org, 2022. QGIS Geographic Information System. QGIS Association. http://www.qgis.org.

Reilinger, R., McClusky, S., Vernant, P., Lawrence, S., Ergintav, S., Cakmak, R., Ozener, H., Kadirov, F., Guliev, I., Stepanyan, R., Nadariya, M., Hahubia, G., Mahmoud, S., Sakr, K., ArRajehi, A., Paradissis, D., Al-Aydrus, A., Prilepin, M., Guseva, T., Evren, E., Dmitrotsa, A., Filikov, S.V., Gomez, F., Al-Ghazzi, R., Karam, G., 2006. GPS constraints on continental deformation in the Africa-Arabia-Eurasia continental collision zone and implications for the dynamics of plate interactions. J. Geophys. Res., 111, 1-26. https://doi.org/10.1029/2005JB004051.

Reilinger, R., McClusky, S., Paradissis, D., Ergintav, S., Vernant, P., 2010. Geodetic constraints on the tectonic evolution of the Aegean region and strain accumulation along the Hellenic subduction zone. Tectonophysics, 488, 22–30. https://doi.org/10.1016/j.tecto.2009.05.027.

Ricou, L.-E., Dercourt, J., Geyssant, J., Grandjacquet, C., Lepvrier, C., Biju-Duval, B., 1986. Geological constraints on the alpine evolution of the Mediterranean Tethys. Tectonophysics, 123, 83–122. https://doi.org/10.1016/0040-1951(86)90194-0.

Ricou, L.-E., 1994. Tethys reconstructed: plates, continental fragments and their Boundaries since 260 Ma from Central America to South-eastern Asia. Geodinamica Acta, 7, 169–218. https://doi.org/10.1080/09853111.1994.11105266.

Ring, U., Glodny, J., Will, T., Thomson, S., 2010. The Hellenic Subduction System: High-Pressure Metamorphism, Exhumation, Normal Faulting, and Large-Scale Extension. Annu. Rev. Earth Planet. Sci., 38, 45–76. https://doi.org/10.1146/annurev.earth.050708.170910.

Roberts, S., Jackson, J., 1991. Active normal faulting in central Greece: an overview. Geological Society, London, Special Publications, 56, 125–142. https://doi.org/10.1144/GSL.SP.1991.056.01.09.

Roberts, G.P., 1996. Noncharacteristic normal faulting surface ruptures from the Gulf of Corinth, Greece. J. Geophys. Res., 101, 25,255–25,267.

Roberts, G.P., Ganas, A., 2000. Fault-slip directions in central and southern Greece measured from striated and corrugated fault planes: Comparison with focal mechanism and geodetic data. Journal of Geophysical Research, 105, 443-462.

Robertson, A.H.F., Clift, P.D., Degnan, P.J., Jones, G., 1991. Paleogeographical and paleotectonic evolution of the eastern Mediterranean Neotethys. Paleooceanography Paleoclimatology Paleoecology, 87, 289–343.

Robertson, A.H.F., 2006. Contrasting modes of ophiolite emplacement in the Eastern Mediterranean region. In: Gee DG, Stephenson RA (eds) Geol Soc Lond Memoirs, 32, 235–261.

Rodriguez, M., Sakellariou, D., Gorini, C., Janin, A., D'Acremont, E., Le Pourhiet L., Chamot-Rooke, N., Tsampouraki-Kraounaki, K., Morfis, I., Rousakis, G., Henry, P., Lurin, A., Delescluse, M., Briole, P., Rigo, A., Arsenikos, S., Bulois, C., Fernandez-Blanco, D., Beniest, A., Grall, C., Chanier, F., Caroir, F., Dessa, J.-X., Oregioni, D., Nercessian, A., 2023. Evolution of the North Anatolian Fault from a diffuse to a localized shear zone in the North Aegean Sea during the Plio-Pleistocene. Geophysical Journal International, 235, 2614–2639. https://doi.org/10.1093/gji/ggad364

Roussos, N., Lyssimachou, T., 1991. Structure of the Central North Aegean Trough: an active strike-slip deformation zone. Basin Res. 3 (1), 37–46.

Roundoyannis-Tsiambaou, Th., 1984. Etude néotectonique des rivages occidentaux du canal d'Atalanti (Grèce centrale). Thèse 3e cycle, 190 pp. Univ. Paris-Sud, Orsay, France.

Royden, L.H., Papanikolaou, D.J., 2011. Slab segmentation and late Cenozoic disruption of the Hellenic arc. Geochem. Geophys. Geosyst., 12, 1-24. https://doi.org/10.1029/2010GC003280.

Saccani, E., Beccaluva, L., Coltorti, M., Siena, F., 2004. Petrogenesis and tectono-magmatic significance of the Albanide-Hellenide subpelagonian ophiolites. Ofioliti, 29, 73–93.

Saccani, E., Photiades, A., Santato, A., Zeda, O., 2008. New evidence for supra-subduction zone ophiolites in the Vardar zone of northern Greece: implications for the tectono-magmatic evolution of the Vardar oceanic ocean. Ofioliti, 33, 65–85.

Sachpazi, M., Galvé, A., Laigle, M., Hirn, A., Sokos, E., Serpetsidaki, A., Marthelot, J.M., Pi Alperin, J.M., Zelt, B., Taylor, B., 2007. Moho topography under central Greece and its compensation by Pn time-terms for the accurate location of hypocenters: The example of the Gulf of Corinth 1995 Aigion earthquake. Tectonophysics, 440, 53-65

Sakellariou, D., Rousakis, G., Kaberi, H., Kapsimalis, V., Georgiou, P., Kanellopoulos, Th., Lykousis, V., 2007. Tectono-sedimentary structure and late Quaternary evolution of the North Evia Gulf basin, Central Greece: preliminary results. Bulletin of the Geological Society of Greece, 40, 1-12. https://doi.org/10.12681/bgsg.16644.

Sakellariou, D., Rousakis, G., Vougioukalakis, G., Ioakim, Ch., Panagiotopoulos, I., Morfis, I., Zimianitis, E., Athanasoulis, K., Tsampouraki-Kraounaki, K., Mpardis, D., 2016. Deformation pattern in the western North Aegean Trough: preliminary results. Bulletin of the Geological Society of Greece, 50, 1-10. https://doi.org/10.12681/bgsg.11708.

Sakellariou, D., Tsampouraki-Kraounaki, K., 2019. Plio-Quaternary extension and strike-slip tectonics in the Aegean. In: J. Duarte (Ed.): Transform Plate Boundaries and Fracture Zones, Chapter 14, p. 339-374, https://doi.org/10.1016/B978-0-12-812064-4.00014-1**,** ELSEVIER, 2019, ISBN: 978-0-12-812064-4.

Savvaidis, A., Smirnov M.Y., Tranos, M.D., Pedersen, L.B., Chouliaras, G., 2012. The seismically active Atalanti fault in Central Greece: A steeply dipping fault zone imaged from magnetotelluric data. Tectonophysics, 554-557, 105-113.

Schmid, S.M., Fügenschuh, B., Kounov, A., Matenco, L., Nievergelt, P., Oberhänsli, R., Pleuger, J., Schefer, S., Schuster, R., Tomljenović, B., 2019. Tectonic units of the Alpine collision zone between Eastern Alps and Western Turkey. Gondwana Res., 78, 308-374.

Sengör, A.M.C., 1979. The North Anatolian transform fault: its age, offset and tectonic significance. JL geol. Soc. Lond., 136, 269-282.

Sengor, A.M.C., Yilmaz, Y., 1981. Tethyan evolution of Turkey: a plate tectonic approach. Tectonophysics, 75, 181-241.

Sengör, A.M.C., Canitez, N., 1982. The North Anatolian fault, in: Berchemer, H., Hsü, K. (Eds.), Geodynamics Series. American Geophysical Union, Washington, D. C., pp. 205–216. https://doi.org/10.1029/GD007p0205.

Sengör, A.M.C., Tüysüz, O., İmren, C., Sakınç, M., Eyidoğan, H., Görür, N., Le Pichon, X., Rangin, C., 2005. The North Anatolian Fault: A New Look. Annu. Rev. Earth Planet. Sci., 33, 37–112. https://doi.org/10.1146/annurev.earth.32.101802.120415.

Sharp, I.R., Robertson, A.H.F., 1998. Late Jurassic-Lower Cretaceous oceanic crust and sediments of the Eastern Almopias Zone, NW Macedonia (Greece); implications for the evolution of the eastern ''Internal'' Hellenides. Bull Geol Soc Greece, 30(1), 47–61.

Sharp, I.R., Robertson, A.H.F., 2006. Tectonic-sedimentary evolution of the western margin of the Mesozoic Vardar Ocean: evidence from the Pelagonian and Almopias zones, northern Greece. Geol. Soc. Lond., Spec. Publ., 260 (1), 373-412.

Smith, A.G., Hynes, A.J., Menzies, M., Nisbet, E.G., Price, I., Welland, M.J., Ferrière, J., 1975. The stratigraphy of the Othris mountains, eastern Central Greece: a deformed Mesozoic continental margin sequence. Eclogae Geologicae Helveticae, 68, 463-481.

Sorel, D., 2000. A Pleistocene and still-active detachment fault and the origin of the Corinth-Patras rift, Greece. Geology, 28, 83–86.

Stewart, S.A., 2011. Vertical Exaggeration of Reflection Seismic Data in Geoscience Publications 2006–2010. Marine and Petroleum Geology, 28, 959–65. doi: 10.1016/j.marpetgeo.2010.10.003.

Storchak, D.A., Di Giacomo, D., Bondár, I., Engdahl, E.R., Harris, J., Lee, W.H.K., Villaseñor, A., Bormann, P., 2013. Public Release of the ISC-GEM Global Instrumental Earthquake Catalogue (1900-2009). Seism. Res. Lett., 84, 810-815, doi: 10.1785/0220130034.

Symeonidis, N., 1974. Ein Bemerkenswerter Wirrbeltierfund aus dem Lignit von Atalanti (Phthiotis, Griechenland), Ann. Geol. Pays Hell., 26, 306-314.

Tataris, A., Kounis, G., MaraGoudakis, N., Christodoulou, G., Bizon, G., Tsaïla-Monopolis, ST., Zaronikos, J.N., 1970. Geological map of Thivai at 1:50 000 scale, published by IGME.

Taymaz, T., Jackson, J., McKenzie, D., 1991. Active tectonics of the north and central Aegean Sea. Geophysical Journal International, 106, 433–490. https://doi.org/10.1111/j.1365-246X.1991.tb03906.x.

Taymaz, T., Yilmaz, Y., Dilek, Y., 2007. The geodynamics of the Aegean and Anatolia: Introduction. From Taymaz, T., Yilmaz, Y., Dilek, Y., 2007. The geodynamics of the Aegean and Anatolia. Geological Society, London, Special Publications, 291, 1-16. Doi: 10.1144/SP291.1.

Thiebault, F., 1982. Evolution géodynamique des hellenides externes en Péloponnèse méridional (Grèce). Soc. Geol. Nord, 6.

Tiberi, C., Diament, M., Lyon-Caen, H., King, T., 2001. Moho topography beneath the Corinth Rift area (Greece) from inversion of gravity data. Geophysical Journal International, 145, 797–808. https://doi.org/10.1046/j.1365-246x.2001.01441.x.

U.S. Geological Survey, 2021, Earthquake Lists, Maps, and Statistics, accessed March 09, 2021 at URL https://www.usgs.gov/natural-hazards/earthquake-hazards/lists-maps-and-statistics.

Van Andel, T.H., Perissoratis, C., 2006. Late Quaternary depositional history of the North Evvoikos Gulf, Aegean Sea, Greece. Marine Geology, 232, 157–172. https://doi.org/10.1016/j.margeo.2006.07.004.

van Hinsbergen D.J.J., Zachariasse W.J., Wortel M.J.R., Meulenkamp J.E., 2005a. Underthrusting and exhumation: a comparison between the External Hellenides and the "hot" Cycladic and "cold" South Aegean core complexes (Greece). Tectonics, 24, TC2011. http://dx.doi.org/10.1029/2004TC001692.

van Hinsbergen, D. J. J., Hafkenscheid, E., Spakman, W., Meulenkamp, J.E., Wortel, M.J.R., 2005b. Nappe stacking resulting from subduction of oceanic and continental lithosphere below Greece, Geology, 33, 325–328, doi:10.1130/G20878.1.

van Hinsbergen, D.J.J., Dekkers, M.J., Bozkurt, E., and Koopman, M., 2010. Exhumation with a twist: paleomagnetic constraints on the evolution of the Menderes metamorphic core complex, western Turkey. Tectonics, 29(3): TC3009 doi: 10.1029/2009TC002596.

van Hinsbergen, D.J.J., Torsvik, T.H., Schmid, S.M., Matenco, L.C., Maffione, M., Vissers, R.L.M., Gürer, D., Spakman, W., 2020. Orogenic architecture of the Mediterranean region and kinematic reconstruction of its tectonic evolution since the Triassic. Gondwana Res., 81, 79-229. Doi: 10.1016/j.gr.2019.07.009.

Vanderhaeghe, O., Teyssier, C., 2001. Crustal-scale rheological transitions during late-orogenic collapse. Tectonophysics, 335, 211–228. https://doi.org/10.1016/S0040-1951(01)00053-1.

Vassilakis, E., Royden, L., Papanikolaou, D., 2011. Kinematic links between subduction along the Hellenic trench and extension in the Gulf of Corinth, Greece: A multidisciplinary analysis. Earth and Planetary Science Letters, 303, 108-120.

Vergely, P., 1984. Tectonique des ophiolites dans les Hellenides internes. Conséquences sur l'évolution des régions téthysiennes occidentales. Thèse Université Paris sud Orsay, 2 vol, 250 et 411 pp.

Walcott, C.R., White, S.H., 1998. Constrains on the kinematic of post-orogenic extension imposed by stretching lineations in the Aegean region. Tectonophysics, 298, 155-175.

Zelt, B.C., Taylor, B., Sachpazi, M., Hirn, A., 2005. Crustal velocity and Moho structure beneath the Gulf of Corinth, Greece. Geophys. J. Int., 162, 257-268.

Figure Captions

Figure 1: **A)** Simplified structural map of Eastern Mediterranean (modified after Hejl *et al.*, 2010 and Jolivet *et al.*, 2013). GPS horizontal velocities from McClusky *et al.* (2000); Taymaz *et al.* (2007) and Müller *et al.* (2013). Aegean volcanic arcs from Vassilakis *et al.* (2011). **B)** Map of the main Hellenic units constituting the Greece mainland (modified after Ferrière *et al.*, 2012). The study area, the North Evia domain, is located in the red square. **C)** Schematic cross-section (not to scale) from Parnassos Mount to North Evia Island through the North Evia Gulf, located by an orange line on the map. IZTF: Internal Zones Thrust Front.

Figure 2: Bathymetric and topographic map of the North Evia domain, respectively from EMODnet (horizontal resolution of 125 m), and SRTM30 network (Farr *et al.*, 2007). Faults compilation realised from previous studies (Eliet and Gawthorpe, 1995; Ganas, 1997; Palyvos *et al.*, 2006; Kranis, 2007; Sakellariou *et al.*, 2007; Kilias *et al.*, 2008; Evelpidou *et al.*, 2012; Savvaidis *et al.*, 2012; Sakellariou *et al.*, 2016; Porkoláb *et al.*, 2019; Mouslopoulou *et al.*, 2022). Faults: AMFS: Atalanti–Martino Fault Segments; Ar: Arkitsa fault segment; HFZ: Hyampolis Fault Zone; KEFZ: KEchriae Fault Zone; KFS: Kallidromon Fault Segments; KVAFS: Kamena Vourla–Arkitsa Fault System; MFZ: Melouna Fault Zone; NAF: North Anatolian Fault; PoF: Politika Fault; PPFZ: Prokopi–Pilion Fault Zone; SIFZ: Sperchios–Ipati Fault Zone. North Evia Gulf: Central Basin (CB), Eastern Basin (EB), Western Basin (WB). Li: Lichades peninsula; M: Malesina Peninsula; MG: Maliakos Gulf; R: Reginio Basin; T: Telethrion mounts.

Figure 3: Location map of WATER Sparker data (black lines) and airgun data from Sakellariou *et al.* (2007) with bathymetry and location of presented profiles. AC: Artemision Channel; CB: Central Basin; EB: Eastern Basin; Li: Lichades peninsula; MG: Maliakos Gulf; NEG: North Evia Gulf; OC: Oreoi Channel; PG: Pagasitikos Gulf; WB: Western Basin.

Table 1: Seismic units and seismic facies identified from the WATER surveys. Unit A and Unit B are represented on the profiles with light colours in the areas where direct correlation does not exist.

Figure 4: Structural map of the study area from marine seismic data (Sparker data from WATER surveys and single-channel airgun data from Sakellariou *et al.*, 2007), and compilation of published faults (Eliet and Gawthorpe, 1995; Ganas, 1997; Palyvos *et al.*, 2006; Kranis, 2007; Kilias *et al.*, 2008; Evelpidou *et al.*, 2012; Savvaidis *et al.*, 2012; Sakellariou *et al.*, 2016; Porkoláb *et al.*, 2019 ; Mouslopoulou *et al.*, 2022). Geological background onland is simplified from 1:50,000 maps of Greece (IGME: Marinos *et al.*, 1957, 1963, 1967; Papastamatiou *et al.*, 1960, 1962; Maratos *et al.*, 1965, 1967; Tataris *et al.*, 1970; Katsikatsos *et al.*, 1978, 1978b, 1980, 1981; Parginos *et al.*, 2007). The offshore area coloured in brown between Skiathos and Evia is the Evia–Skiathos Ridge, a new structure detailed below in this study (section 4.2.4.). AC : Artemision Channel ; AMFS: Atalanti–Martino Fault Segments; APFS: Aedipsos–Politika Fault System; Ar: Arkitsa fault segment; At: Atalanti fault segment; CB: Central Basin; CBFS: Central Basin Fault System; EB: Eastern Basin; HFZ: Hyampolis Fault Zone; KEFZ: KEchriae Fault Zone; KFS: Kallidromon Fault Segments; Kn: Knimis; KVAFS: Kamena Vourla–Arkitsa Fault System; Li: Lichades peninsula; M: Malesina peninsula; MFZ: Melouna Fault Zone; MG: Maliakos Gulf; NAF: North Anatolian Fault; OC: Oreoi Channel; PFS: Parnassos Fault System; PoF:

Politika Fault; PPFZ: Prokopi–Pilion Fault Zone; R: Reginio Basin; SIFZ: Sperchios–Ipati Fault Zone; SSF: South Skopelos Fault; T: Telethrion; TEFZ: Telethrion Fault Zone; WB: Western Basin; WFZ: Western Fault Zone.**Table 2**: Table of the 46 chosen faults, their characteristics and their location are indicated. See the text for details. AC: Artemision Channel; CB: Central Basin; EB: Eastern Basin; Li: Lichades peninsula; OC: Oreoi Channel; PG: Pagasitikos Gulf; WB: Western Basin.

Figure 5: Location map of the main faults, listed in Table 2. AC: Artemision Channel; CB: Central Basin; EB: Eastern Basin; Li: Lichades peninsula; OC: Oreoi Channel; PG: Pagasitikos Gulf; WB: Western Basin.

Figure 6: Structural map of the Lichades Zone and its vicinity. The red star indicates the ~500 000 years old calc-alkaline volcanic islands. KFS: Kallidromon Fault Segment; Kn: Knimis mounts; KVAFS: Kamena Vourla–Arkitsa Fault System; Li: Lichades peninsula; MG: Maliakos Gulf; MoF: Molos Fault; OC: Oreoi Channel; OrF: Oreoi Fault; R: Reginio Basin; SIFZ: Sperchios–Ipati Fault Zone; WB: Western Basin.

Figure 7: Sparker seismic profile WAT17_124 showing the Lichades shear and fault segments of the Lichades Zone. Location in Figure 6. The green triangles and vertical line indicate the location of an anticline axis. OrF: Oreoi Fault; UA: Unit A; US: Upper Sequence. Multiples are shaded in light grey.

Figure 8: Sparker seismic profile WAT17_149 showing deformation within the Upper Sequence and its southward thickening. Location in Figure 6. Onlap and toplap terminations are indicated by blue arrows. Li3 corresponds to the fault listed in Table 2 and located in Figure 5. M: first multiple of the sea floor; US: Upper Sequence.

Figure 9: Structural map of the North Evia Gulf established from WATER and Sakellariou *et al.* (2007) surveys. The profiles presented below are indicated in red. Major faults are represented by thick black lines. The hatched area corresponds to the intensely deformed Aedipsos Platform. AMFS: Atalanti–Martino Fault Segments; APFS: Aedipsos–Politika Fault System; Ar: Arkitsa fault; At: Atalanti fault; CB: Central Basin; CBFS: Central Basin Fault System; EB: Eastern Basin; HFZ: Hyampolis Fault Zone; KEFZ: Kechriae Fault Zone; KVAFS: Kamena Vourla–Arkitsa Fault System; Li: Lichades peninsula; MFZ: Melouna Fault Zone; PoF: Politika Fault; PPFZ: Prokopi–Pilion Fault Zone; T: Telethrion; TEFZ: Telethrion Fault Zone; WB: Western Basin; WFZ: Western Fault Zone.

Figure 10: Sparker seismic profile WAT17_221 showing the Western Fault Zone (WFZ), the eastern part of the WB, and the Aedipsos Platform. Location on Figure 9. The focal mechanism is from the International Seismological Centre catalogue (Storchak *et al.*, 2013; Di Giacomo *et al.*, 2018) and has been projected following the profile orientation. Multiples are shaded in light grey. The numbers 1, 2 and 3 indicate the three zones of the Lichades Platform (see the text for details). WB4 and WB7 correspond to the faults listed in Table 2 and located in Figure 5. UA: Unit A; UB: Unit B; US: Upper Sequence.

Figure 11: Airgun seismic profile 4_3 from Sakellariou *et al.* (2007) showing the rift structure in the western part of the CB. Location on Figure 9. CB1 and CB2 are two major faults listed in Table 2 and located in Figure 5. APFS: Aedipsos–Politika Fault System; CBFS: Central Basin Fault System; M: first multiple of the sea floor; MTD: Mass Transport Deposit; UA: Unit A; UB: Unit B; US: Upper Sequence.

Figure 12: Sparker seismic profile WAT17_203 and interpretation showing the eastern part of the Central Basin Fault System (CBFS). Location on Figure 9. CB10 is one of the faults listed in Table 2 and located in Figure 5. UA: Unit A; UB: Unit B; US: Upper Sequence.**Figure 13**: Sparker seismic profile WAT17_174 showing the Melouna Fault Zone (MFZ) separating Larymna and Kandili sub-basins. Location in Figure 9. UA: Unit A; UB: Unit B; URU: Undulated Reflector Unit; US: Upper Sequence. Asterisk indicates the major fault, referenced as EB4 in Table 2 and Figure 5.

Figure 14: Sparker seismic profile WAT17_085 showing the main faults observed in the Oreoi Channel. Location in Figure 3. OC3 corresponds to the fault listed in Table 2 and located in Figure 5. UA: Unit A; UB: Unit B; US: Upper Sequence.

Figure 15: Structural map of the Skiathos and Skopelos basins established from WATER surveys. The profiles presented below are indicated in red. NAF: North Anatolian Fault; SSF: South Skopelos Fault.

Figure 16: Sparker seismic profile WAT17_019 illustrating the Skiathos Basin with few NW-dipping normal faults (in red), the Evia-Skiathos Ridge and other buried basement ridges. Location in Figures 3 and 15. SkiB1 is listed in Table 2 and located in Figure 5. S6: 6th clinoform sequence identified in the Artemision Channel; US: Upper Sequence.

Figure 17: Sparker seismic profiles WAT17_059, WAT17_054 and WAT17_053 illustrating the Skiathos Basin, the Evia-Skiathos Ridge and SE-dipping normal faults. Location in Figures 3 and 15. SkiB2 is the second fault in the Skiathos Basin detailed in Table 2 and located in Figure 5. S6: 6th clinoform sequence identified in the Artemision Channel; US: Upper Sequence.

Figure 18: Sparker seismic profile WAT17_013 illustrating the Skopelos Basin and the South Skopelos Fault (SSF). Location in Figures 3 and 15.

Figure 19: Structural sketch map of N.V Evia with reported main faults from the NOA fault database (Ganas *et al.*, 2013) including our fault measurements reported on stereonets (equal-area, lower hemisphere). Thicker lines on stereonets correspond to major fault planes (over several metres of observed displacement), dashed lines correspond to bedding planes.

Figure 20: **A)** Structural map and location of historical earthquakes (Mw > 3) from 550 *BC* to 2011 (black circles) from the catalogue of Aristotle University of Thessaloniki. **B)** Earthquakes instrumentally recorded from 1970 to 2020 (coloured circles) from the catalogues of USGS Latest Earthquakes and the International Seismological Centre (Storchak *et al.*, 2013; Di Giacomo *et al.*, 2018) AC: Artemision Channel; Li: Lichades peninsula; MFZ: Melouna Fault Zone; NAF: North Anatolian Fault; NEG: North Evia Gulf; OC: Oreoi Channel; PG: Pagasitikos Gulf; SSF: South Skopelos Fault; WFZ: Western Fault Zone.

Figure 21: Structural map of the North Evia domain with a compilation of the main focal mechanisms with a strike-slip component from the International Seismological Centre (Storchak *et al.*, 2013; Di Giacomo *et al.*, 2018) and Global Project Centroid Moment Tensor (Ekström *et al.*, 2012) catalogues and the microseismicity study of Kiratzi (2002). Black beach balls indicate earthquakes located between 0 and 15 km, and grey beach balls for earthquakes located between 15 and 30 km. P-axis and T-axis are respectively marked in red and green.

AB: Almiros Basin; AC: Artemision Channel; Li: Lichades peninsula; M: Malesina peninsula; NAF: North Anatolian Fault; NAT: North Aegean Trough; NEG: North Evia Gulf; OC: Oreoi Channel; R: Reginio Basin; SSF: South Skopelos Fault.

Figure 22: Location of strike-slip corridors deduced from focal mechanisms and fault analysis. AB: Almiros Basin; AC: Artemision Channel; APFS: Aedipsos–Politika Fault System; CBFS: Central Basin Fault System; KAMFS: Kallidromon–Atalanti–Martino Fault System; KVAFS: Kamena Vourla–Arkitsa Fault System; Li: Lichades peninsula; M: Malesina peninsula; MFZ: Melouna Fault Zone; NAF: North Anatolian Fault; NAT: North Aegean Trough; OC: Oreoi Channel; OrF: Oreoi Fault; PPFZ: Prokopi–Pillion Fault Zone; R: Reginio Basin; SB: Sperchios Basin; SSF: South Skopelos Fault.

Seismic units	Seismic facies		Geometry	Continuity	Frequency	Amplitude
Upper Sequence	SF1	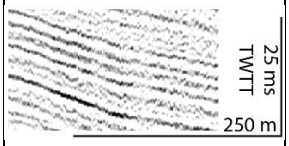	Parallel to sub-parallel	High	High	Moderate
	SF2	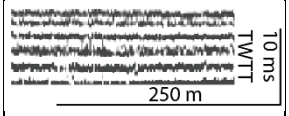	Parallel to sub-parallel	High	High	High
	SF3	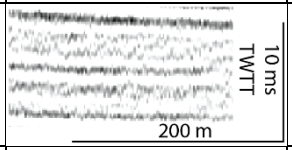	Parallel to sub-parallel	Moderate	High	Low
Unit A	SF2	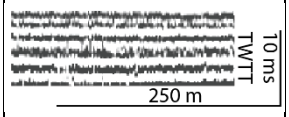	Parallel to sub-parallel	High	High	High
	SF4	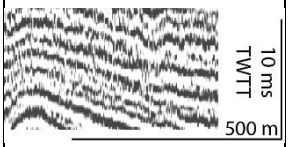	Parallel to sub-parallel	Moderate to high	High	High
	SF5	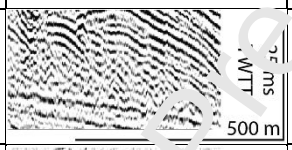	Chaotic / Undulations	Low	High	High
Unit B	SF6		Parallel to sub-parallel	Low to moderate	High	Low to moderate
	SF7 ~SF3	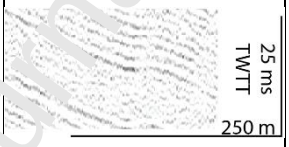	Parallel to sub-parallel	Moderate	High	Low
	SF8	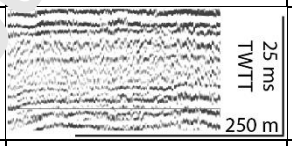	Parallel to sub-parallel	Moderate	Moderate	Low to moderate
	SF9		Parallel / Locally inclined	High	High	Low to moderate

Table 1: Seismic units and seismic facies identified from the WATER surveys data analysis. Unit A and Unit B are represented in the profiles with light colours in the areas where direct correlation does not exist.

Table 2: Table of 46 selected faults (location in Figure 5). The Holocene slip rates are estimated from offset of the base of the US. The depth-conversions consider a 1500 $m \cdot s^{-1}$ velocity in the water column and an estimation of 1800 $m \cdot s^{-1}$ in the US. See the text for details. nd: not determinable.

Area	Fault code	Mean dip direction	Youngest throw (m)	Youngest throw (ms)	Age	US basis offset (m)	US basis offset (ms)	Holocene slip rate (mm/yr)
Lichades Zone	Li1	NNE	9	10	Pre-US	0	0	0
	Li2	S	3.6	4	Pre-US	0	0	0
	Li3	N	5.4	6	Syn-US	5.4	6	0.46
	Li4	S	4.5	5	Syn-US	4.5	5	0.38
	Li5	SSW	2.7	3	Syn-US	2.7	3	0.23
	Li6	SSE	4.5	5	Pre-US	0	0	0
	Li7	SSW	3.6	4	Syn-US	3.6	4	0.31
	Li8	N	9	12	Post-US	13.5	15	1.15
	Li9	S	4.5	5	Pre-US	0	0	0
	Li10	NNW	6	8	Post-US	9	10	0.77
Western Basin	WB1	N	3.4	6	Pre-US	0	0	0
	WB2	N	20.	23	Pre-US	0	0	0
	WB3	NNW	1.8	2	Syn-US	1.8	2	0.15
	WB4	N	3.75	5	Post-US	12.6	14	1.08
	WB5	S	2.25	3	Post-US	5.4	6	0.46
	WB6	N	7.5	10	Post-US	18	20	1.54
	WB7	S	6.75	9	Post-US	19.8	22	1.69
	WB8	N	13.5	15	Pre-US	0	0	0
Central Basin	CB1	SSE	55.5	74	Post-US	82.8	92	7.08
	CB2	N	52.5	70	Post-US	63	70	5.38
	CB3	N	22.5	25	Pre-US	0	0	0
	CB4	N	13.5	15	Pre-US	0	0	0
	CB5	NNW	4.5	6	Post-US	15.3	17	1.31
	CB6	NNE	41.25	55	Post-US	63	70	5.38
	CB7	SW	63.75	85	Post-US	76.5	85	6.54

	CB8	NNE	4.5	6	Post-US	18	20	1.54
	CB9	NNW	15	20	Post-US	20.7	23	1.77
	CB10	N	7.5	10	Post-US	13.5	15	1.15
	CB11	N	18	20	Pre-US	0	0	0
	CB12	NNE	16.2	18	Pre-US	0	0	0
Eastern Basin	EB1	SW	4.5	6	Post-US	6.3	7	0.54
	EB2	SW	13.5	15	Pre-US	0	0	0
	EB3	NE	6.3	7	Pre-US	0	0	0
	EB4	SSW	3.6	4	Syn-US	3.6	4	0.31
	EB5	NNE	9	10	Pre-US	0	0	0
Oreoi-Artemision Channel	OC1	NNW	13.5	15	Pre-US	0	0	0
	OC2	NNW	6.3	7	Pre-US	0	0	0
	OC3	NNW	2.25	3	Post-US	6.3	7	0.54
Skiathos Basin	SkiB1	NW	13.5	15	Pre-S6	0	0	0
	SkiB2	SE	3.6	4	Syn-S6	0	0	0
Skopleos Basin	SkoB1	NW	nd	nd	Post-US	nd	nd	nd
	SkoB2	NNW	45	60	Post-US	nd	nd	nd
	SkoB3	NE	45	60	Post-US	nd	nd	nd
	SkoB4	S	3.75	5	Post-US	nd	nd	nd
	SkoB5	NW	45	60	Post-US	nd	nd	nd
	SkoB6	SE	30	40	Post-US	nd	nd	nd

Declaration of interests

☒The authors declare that they have no known competing financial interests or personal relationships that could have appeared to influence the work reported in this paper.

☐The authors declare the following financial interests/personal relationships which may be considered as potential competing interests:

Highlights:

- New seismic profiles in the western prolongation of North Anatolian Fault
- Mapping offshore fault networks in the North Evia region, Central Greece
- Evidence for a new basin between Sporades Islands and North Evia: Skiathos Basin
- Active strike-slip displacements along NW-SE and NE-SW striking faults